

Joint Spatial and Spectral Hybrid Precoding for Multi-User MIMO-OFDM Systems

Navid Reyhanian, Reza Ghaderi Zefreh, Parisa Ramezani, and Emil Björnson, *Fellow, IEEE*

Abstract—The deployment of millimeter wave (mmWave) technology is pivotal for next-generation networks, providing dramatically increased available bandwidth. mmWave multiple-input multiple-output (MIMO) systems cannot rely solely on digital precoding due to hardware constraints. Instead, hybrid precoding, which combines digital and radio frequency (RF) techniques, has emerged as a potential alternative. This approach strikes a balance between performance and cost, addressing the limitations of signal mixers and analog-to-digital converters in mmWave systems. mmWave systems are designed to function in wideband channels with frequency selectivity, necessitating the use of orthogonal frequency-division multiplexing (OFDM) to mitigate dispersive channels. However, OFDM faces several practical challenges. First, it suffers from a high peak-to-average power ratio (PAPR) due to the linear combination of subcarriers. Second, it suffers from out-of-band (OOB) emissions due to the sharp spectral transitions of OFDM subcarriers and windowing-induced spectral leakage. Furthermore, phase shifter (PS) impairments at the RF transmitter precoder and the user combiner represent an inherent limitation in practical mmWave systems, leading to phase errors. This work addresses these practical challenges.

We study the problem of robust digital-RF precoding optimization for the downlink sum-rate maximization in hybrid multi-user (MU) MIMO-OFDM systems under maximum transmit power, PAPR, and OOB emission constraints. The formulated maximization problem is non-convex and difficult to solve. We propose a weighted minimum mean squared error (WMMSE) based block coordinate descent (BCD) method to iteratively optimize digital-RF precoders at the transmitter and digital-RF combiners at the users. Low-cost and scalable optimization approaches are proposed to efficiently solve the BCD subproblems. Extensive simulation results are conducted to demonstrate the efficiency of the proposed approaches and exhibit their superiority relative to well-known benchmarks.

Index Terms—Millimeter wave technology, hybrid precoding, MU-MIMO-OFDM, phase errors, block coordinate descent, alternating direction method of multipliers.

I. INTRODUCTION

MILLIMETER wave (mmWave) communication is a promising solution to address the bandwidth shortage in next-generation wireless systems [1]. Despite the higher propagation losses at mmWave frequencies compared to conventional sub-6 GHz bands, the smaller wavelength enables the deployment of large-scale antenna arrays at the transceivers, facilitating the use of massive multiple-input multiple-output (MIMO) technology. Massive MIMO leverages these multiple

N. Reyhanian was with the Department of Electrical Engineering, University of Minnesota, Minneapolis, MN, USA 55455. He is now with Cisco Systems, Milpitas, CA, USA 95035 (email: navid@umn.edu).

R.G. Zefreh is Independent Researcher, Shiraz, Fars, Iran (email: r.ghaderi@alumni.iut.ac.ir).

P. Ramezani and E. Björnson are with the Department of Computer Science, KTH Royal Institute of Technology, Stockholm, Sweden (email: {parram,emilbj}o}@kth.se).

antennas at both the transmitter and receiver to transmit and receive multiple beamformed data streams simultaneously, thereby overcoming poor propagation characteristics, enhancing data rates through spatial multiplexing, and improving reliability via spatial diversity. Massive MIMO is particularly well suited for multi-user MIMO (MU-MIMO), where one serves multiple users simultaneously on the same spectrum and needs to control the inter-user interference through beamforming.

Fully-digital beamforming, which requires a separate radio frequency (RF) chain for each antenna, introduces impractical hardware complexity and excessive power consumption in large-scale arrays. To address this, a hybrid phase-shifter (PS) based digital-RF beamforming architecture is adopted, combining a high-dimensional RF beamformer implemented via simple PSs with a low-dimensional digital beamformer [1]–[3]. This approach strikes a balance between performance and hardware efficiency, allowing hybrid beamforming to approach the performance of fully-digital schemes.

However, mmWave systems often operate over wideband channels, where frequency selectivity poses a new challenge. Hybrid beamforming in such frequency-selective channels, typically implemented with orthogonal frequency division multiplexing (OFDM), requires designing a shared RF beamformer across all subcarriers, while the digital beamformer is optimized on a per-subcarrier basis [4]. This differs from flat-fading channel designs and introduces additional complexity in maintaining performance across multiple subcarriers.

Additionally, OFDM’s challenges such as high peak-to-average power ratio (PAPR) and out-of-band (OOB) emissions must be addressed [5]. High PAPR impacts digital-to-analog converters (DACs) and power amplifiers (PAs), causing signal distortion and spectral regrowth [6]. These nonlinearities degrade both in-band and adjacent channel performance, which is particularly critical in mmWave systems due to their wide bandwidth. Thus, careful integration of PAPR reduction techniques into hybrid beamforming design is necessary to optimize mmWave MIMO-OFDM systems for future wireless networks. Moreover, one of the challenges in deploying OFDM, particularly in mmWave MIMO systems, is its high OOB emissions, which can interfere with adjacent systems and degrade their communication performance [7]. This problem is exacerbated in scenarios such as access points (APs) that require higher average transmit power to provide adequate coverage. To address interference in adjacent channels, standardized wireless systems enforce stringent OOB emission limits, typically evaluated using metrics such as the adjacent channel leakage ratio (ACLR) and spectral emission mask [8].

A. Related Work

Precoding for hybrid systems is widely studied in the literature, e.g., [1], [2], [4]. In partially-connected hybrid systems, each antenna links to one RF chain, leading to manageable implementation complexity. In fully-connected systems, each antenna connects to all RF chains, enhancing flexibility but increasing complexity and insertion losses. The performance of hybrid precoding for partially-connected and fully-connected single-user (SU) MIMO-OFDM systems is studied in [1], where it is shown that precoding using the fully-connected architecture can achieve spectral efficiency very close to that of fully-digital beamforming. To optimize the RF precoding at the transmitter, which is a non-convex problem due to the unit modulus constraints of phase shifts, Riemannian conjugate gradient (RCG) methods are considered and commonly deployed, e.g., [2], [4]. However, hybrid precoding systems often face the additional challenge of high PAPR, which limits practical implementation efficiency.

Different methods have been developed to handle the non-convex PAPR constraint [9]–[14]. In particular, the PAPR constraint is convexified in [9], [12] using the previous iterate for the ℓ_2 -norm in the PAPR calculation. A compensation signal is considered to be transmitted with the original sequence such that the aggregated signal has a smaller PAPR and remains unclipped in [10]. In [11], a constant transmit power is used; therefore, the PAPR constraint simplifies to clipping (limiting the amplitude of time domain signals). While the PAPR reduction in the beamforming process is studied for OFDM systems with deterministic symbols, e.g., [9]–[12], the PAPR reduction in minimum mean squared error (MMSE) based precoding methods for MU-MIMO-OFDM systems has not been studied.

Spectral precoding is an effective technique to suppress OOB emissions. A least-squares notching spectral precoder to suppress OOB emissions at specific frequencies is proposed in [15] that minimizes the Euclidean distance between the spectrally precoded and original data vectors. This approach aims to null OOB emissions at specified frequencies while preserving the integrity of the in-band signal. Mask-compliant spectral precoder schemes have been proposed in [16]–[18], which adhere to predefined spectral emission upper limits instead of nulling OOB at specific frequency points. The joint suppression of PAPR and OOB radiation for SU-MIMO-OFDM systems is explored in [7], where a constant PAPR is assumed and OOB emissions are minimized.

Transmit signals are typically precoded using two independently designed spectral and spatial precoders for SU systems, e.g., [8], [15]. However, spectral precoding can negatively impact the overall system throughput, particularly in high data-rate MU-MIMO-OFDM systems. This performance degradation arises from malforming the spatially-precoded signals caused by spectral precoding, which strengthens interference and reduces the system's spectral efficiency. The joint spatial and spectral precoding for MU-MIMO-OFDM is studied in [19], where zero-forcing (ZF) and maximum-ratio transmission (MRT) precoding methods are proposed to manage interference at users. ZF precoding performs badly when the

signal-to-noise ratio (SNR) is low because it attenuates the desired signal too strongly, while MRT struggles with MU interference since it primarily optimizes the SNR for a single user but is inadequate in mitigating inter-user interference. MMSE [20] and weighted MMSE (WMMSE) [21] precoding methods effectively balance noise and interference, making them preferable for practical MU-MIMO scenarios [22].

PS impairments are unavoidable hardware limitations in practical mmWave hybrid beamforming systems, arising from manufacturing imperfections, low-quality RF components, and device aging. This leads to random phase and gain errors that can severely degrade system performance. These impairments are typically modeled as random deviations from ideal PS responses, with phase errors following Gaussian distributions [23]–[27]. Recent works have addressed these challenges through different approaches: Li *et al.* [26] propose robust hybrid beamforming design using alternating optimization with outage probability constraints under PS error uncertainty, while [25] develops a novel method that estimates the downlink equivalent channel directly (which inherently captures the effects of imperfect PSs) and designs digital precoders based on this estimated channel rather than relying on channel reciprocity, thereby achieving robustness while reducing training overhead.

Although the areas above have been partially studied in isolation, they need to be considered jointly within a unified framework to address the resulting challenges. The main focus of this paper is to design a robust joint spatial and spectral precoding framework for hybrid partially-connected MU-MIMO-OFDM systems.

B. Our Contributions

In this paper, we study a robust hybrid precoding design for MU-MIMO-OFDM systems with partially-connected transmitter structures under PAPR, clipping, and OOB emission constraints. The key contributions of this paper are as follows:

- We formulate the problem of user sum-rate maximization through the optimization of digital and RF precoders at the transmitter, digital and analog combiners at the users. This joint optimization problem is non-convex with respect to all variables, making it difficult to solve. We propose a WMMSE-based block coordinate descent (BCD) algorithm to efficiently solve the problem by alternatively optimizing different variable blocks.
- The subproblem with respect to the digital precoder comprises of a convex objective function subject to one non-convex and three convex constraints. The non-convex constraint arises from the PAPR limitation, while the convex constraints are obtained from the maximum transmit budget, notching spectrum at specific frequencies, and signal amplitude clipping. User symbols are random; therefore, digital precoders are designed such that the above constraints are satisfied with high probability. We show that the non-convex constraint can be relaxed since the WMMSE method promotes precoders with low PAPR (adjustable with the oversampling factor). To solve the large-dimensional subproblem with three

constraints, we decompose it and propose a low-cost and scalable alternating direction method of multipliers (ADMM) to sequentially solve three smaller problems for which solutions can be obtained via closed-forms or bisection searches.

- The subproblems with respect to partially-connected RF precoder and fully (or partially)-connected analog combiners at the transmitter and users, respectively, are non-convex, although the objective function is convex with respect to these variable blocks. This non-convexity is due to the fact that there is one unit modulus constraint for each PS. To optimize the PS phase shifts at the transmitter and users, we deploy a coordinate descent method. We keep all PS values fixed except one that is to be updated. For each PS at the transmitter or a user, we derive a closed-form update rule. In the appendix, for comparison purposes, we also propose a Riemannian manifold method with Polak-Ribiere step-size to optimize PS values and ensure a monotonic decrease in the objective function, and solve the problem to a local optimal solution. In addition, we consider the scenario where PSs are impaired and exact phase shift adjustments are hard to achieve. Robust schemes for PS value optimizations with closed-form solutions at the transmitter and users are proposed that maximize the expected sum-rate in the presence of random phase errors. Finally, closed-form solutions are derived for digital combiners at the users.
- In the proposed BCD algorithm, the above blocks are optimized alternatively with the Gauss-Seidel rule until all blocks converge. The convergence of the proposed method to solve each subproblem is theoretically supported, as well as the overall BCD approach. Extensive simulation results are given to demonstrate the efficiency of the proposed algorithms in reducing OOB emissions and enhancing achievable rates relative to well-known existing methods.

The rest of this paper is organized as follows. We explain the system model in Section II and then present the problem formulation in Section III, where the constraints are also reformulated to manage inherent complexities. A detailed solution illustration, algorithmic decomposition, and our corresponding optimization methods are described in Section IV. Extensive simulation results are provided and discussed in Section V. We conclude this paper in Section VI.

II. SYSTEM MODEL

In this section, we define and study different components of the system model.

1) *fully-digital Systems*: We consider the downlink of a MIMO-OFDM system where an AP is equipped with N_t transmit antennas and serves K users over S subcarriers. Let $\mathcal{S} = \{-S/2, \dots, -1, 1, \dots, S/2\}$ be the set of all subcarriers. Each user is equipped with N_r receive antennas and is scheduled on all subcarriers. Let $\mathbf{V}_k^s \in \mathbb{C}^{N_t \times n_k}$ denote the precoding matrix that the AP uses to transmit n_k data streams to user k per subcarrier. Let $\boldsymbol{\omega}_k^s \in \mathbb{C}^{n_k \times 1}$ represent the transmitted signal for user k on subcarrier s . The transmitted

symbol vector is treated as circularly symmetric complex Gaussian variable satisfying $\mathbb{E}[\boldsymbol{\omega}_k^s \boldsymbol{\omega}_k^{s^H}] = \mathbf{I}_{n_k}$.

Assuming a linear channel model, the received signal $\mathbf{y}_k^s \in \mathbb{C}^{N_r \times 1}$ at user k on subcarrier s can be written as

$$\mathbf{y}_k^s = \mathbf{H}_k^s \sum_{j=1}^K \mathbf{V}_j^s \boldsymbol{\omega}_j^s + \mathbf{n}_k^s,$$

where $\mathbf{H}_k^s \in \mathbb{C}^{N_r \times N_t}$ represents the channel matrix from the AP to user k on subcarrier s , and $\mathbf{n}_k^s \in \mathbb{C}^{N_r \times 1}$ denotes the additive white complex Gaussian noise with distribution $\mathcal{CN}(\mathbf{0}, \sigma_{\text{noise},k}^{s^2} \mathbf{I}_{N_r})$.

We assume that the signals for different users and different subcarriers are independent from each other and from the receiver noise. In this paper, we treat interference as noise and consider a linear receiving strategy. The estimated signal at user k on subcarrier s is $\hat{\boldsymbol{\omega}}_k^s = \mathbf{U}_k^{s^H} \mathbf{y}_k^s$, where $\mathbf{U}_k^s \in \mathbb{C}^{N_r \times n_k}$ is the receive combining matrix for user k on subcarrier s .

2) *Hybrid Analog-Digital Systems*: Here, the AP is equipped with both digital and RF precoders. Similar to the linear model given in the previous section, the received signal $\mathbf{y}_k^s \in \mathbb{C}^{N_r \times 1}$ at user k on subcarrier s can be written as

$$\mathbf{y}_k^s = \mathbf{H}_k^s \mathbf{V}_{\text{RF}} \sum_{j=1}^K \mathbf{V}_j^s \boldsymbol{\omega}_j^s + \mathbf{n}_k^s, \quad (1)$$

where $\mathbf{V}_k^s \in \mathbb{C}^{N_{\text{RF}} \times n_k}$ and $\mathbf{V}_{\text{RF}} \in \mathbb{C}^{N_t \times N_{\text{RF}}}$ denotes the applied phase shift matrix of PSs, and N_{RF} represents the number of RF chains. We consider a partially-connected architecture where each antenna is connected to one RF chain. The N_t antennas are split into N_{RF} disjoint subarrays of equal size. Therefore, each row of \mathbf{V}_{RF} has exactly one non-zero complex element whose absolute value is equal to one. If the a^{th} antenna is connected to the m^{th} RF chain, $\mathbf{V}_{\text{RF}}[a, m] = e^{i\varphi_{am}^t}$ where $i = \sqrt{-1}$ and φ_{am}^t is the applied phase rotation.

In addition to the transmitter, each user is equipped with an analog combining matrix. The decoded signal vector on subcarrier s at the k^{th} user can be expressed as $\hat{\boldsymbol{\omega}}_k^s = \mathbf{U}_k^{s^H} \mathbf{U}_{\text{RF},k}^H \mathbf{y}_k^s$, where $\mathbf{U}_{\text{RF},k} \in \mathbb{C}^{N_r \times N_{\text{RF},k}}$ is the analog combining matrix. Similar to the PS precoding matrix, if the a^{th} antenna is connected to the m^{th} RF chain, $\mathbf{U}_{\text{RF},k}[a, m] = e^{i\varphi_{am}^u}$. We consider an arbitrary (partially or fully-connected) architecture for the combiner matrix of the receiver.

3) *Power Constraint for Hybrid Precoding*: The power budget of the AP is constrained as

$$\sum_{k=1}^K \text{tr}(\mathbf{V}_k^{s^H} \mathbf{V}_{\text{RF}}^H \mathbf{V}_{\text{RF}} \mathbf{V}_k^s) \leq P^s. \quad (2)$$

where $\text{tr}(\cdot)$ denotes the trace operator and P^s is the total power budget of the AP on subcarrier s .

In this paper, along with the traditional power constraint, we will also address the PAPR, clipping, and the spectral shaping constraints in MIMO-OFDM systems.

4) *Clipping Constraint*: The OFDM symbol across a symbol interval T_t in the time domain is defined as [15]

$$x^a(t) = \mathbf{p}^T(t) \mathbf{g}^a, \quad (3)$$

where $\mathbf{p}(t) = [p^{-S/2}(t), \dots, p^{S/2}(t)]^T$ is the transmitted pulse vector with subcarrier modulation and \mathbf{g}^a represents the precoded symbol of OFDM at the a^{th} antenna within the symbol interval. The precoded symbol of the fully-digital system is defined as

$$\mathbf{g}^a = \left[\sum_{k=1}^K \mathbf{V}_k^{-S/2}[a, :] \boldsymbol{\omega}_k^{-S/2} \dots \sum_{k=1}^K \mathbf{V}_k^{S/2}[a, :] \boldsymbol{\omega}_k^{S/2} \right]^T.$$

The OFDM pulse with subcarrier modulation for the s^{th} subcarrier is defined as [8], [15], [18]

$$p^s(t) = e^{\iota 2\pi \frac{s}{T_{\text{sym}}} t} I(t), \quad s \in \mathcal{S}, \quad (4)$$

where $I(t)$ is the indicator function given by $I(t) = 1$ for $-T_g \leq t < T_{\text{sym}}$ and $I(t) = 0$ otherwise, with T_g representing the guard interval duration and T_{sym} the symbol duration. The total duration T_t is given by $T_t = T_{\text{sym}} + T_g$. The rectangular pulse assumption serves as a worst-case analysis for OOB emissions since it exhibits the slowest spectral decay rate compared to other pulses, meaning that any suppression achieved here will likely be even better with band-limited pulses.

The Fourier transform of the OFDM symbol is given by $X^a(f) = \mathbf{o}^T(f) \mathbf{g}^a$, where $\mathbf{o}(f) = [o^{-S/2}(f), \dots, o^{S/2}(f)]^T$ is the frequency-domain representation of the pulse vector with subcarrier modulation. The Fourier transform of $p^s(t)$ in (4) is

$$o^s(f) = T_t e^{-\iota \pi (T_{\text{sym}} - T_g) \left(f - \frac{s}{T_{\text{sym}}} \right)} \text{sinc} \left(\pi T_t \left(f - \frac{s}{T_{\text{sym}}} \right) \right),$$

where the sinc function is defined as $\text{sinc}(x) = \frac{\sin(x)}{x}$.

We discretize (3) at times $t_n = (n - 1)T_{\text{sym}}/\ell S, n \in \{1, \dots, \ell S\}$, where ℓ represents the oversampling factor. If we substitute t_n into (3), we obtain $\mathbf{x}^a[n] = x^a(t_n) = \mathbf{p}^T(t_n) \mathbf{g}^a$. Based on the above equation, we define $\mathbf{F}^{-1} = \{\{e^{\frac{\iota 2\pi s(n-1)}{\ell S}}\}_{s \in \mathcal{S}}\}_{n=1}^{\ell S} \in \mathbb{C}^{\ell S \times S}$. The discrete time-domain OFDM symbol $x^a(t)$ with ℓ times oversampling for the a^{th} antenna ($a = 1, 2, \dots, N_t$) in fully-digital systems is represented as $\mathbf{x}^a = \mathbf{F}^{-1} \mathbf{g}^a \in \mathbb{C}^{\ell S \times 1}$. For hybrid systems, the RF precoder should also be considered in deriving the time domain signals. Let us define the vector of precoded symbols at antenna a as follows:

$$\mathbf{w}^a = \begin{bmatrix} \sum_{k=1}^K \mathbf{V}_{\text{RF}}[a, :] \mathbf{V}_k^{-S/2} \boldsymbol{\omega}_k^{-S/2} \\ \vdots \\ \sum_{k=1}^K \mathbf{V}_{\text{RF}}[a, :] \mathbf{V}_k^{S/2} \boldsymbol{\omega}_k^{S/2} \end{bmatrix}.$$

We have the time domain signal as $\mathbf{x}^a = \mathbf{F}^{-1} \mathbf{w}^a \in \mathbb{C}^{\ell S \times 1}$.

One way of limiting the amplitude of the OFDM signal is clipping. Clipping works by limiting the amplitude of the transmitted signal to a predefined threshold level. When the signal exceeds this threshold, its amplitude is clipped, effectively reducing the peaks. More specifically, the clipping procedure is performed by

$$\hat{\mathbf{x}}^a[n] = \begin{cases} \chi e^{\iota \vartheta[n]}, & |\mathbf{x}^a[n]| > \chi, \\ \mathbf{x}^a[n], & |\mathbf{x}^a[n]| \leq \chi, \end{cases}$$

where $\vartheta[n]$ represents the phase of $\mathbf{x}^a[n]$ for $1 \leq n \leq \ell S$, and χ is the clipping level. It is desired that $|\mathbf{x}^a[n]| \leq \chi$ for $1 \leq n \leq \ell S$ or equivalently $\|\mathbf{x}^a\|_{\infty} \leq \chi$.

5) *PAPR Constraint*: The PAPR constraint refers to the ratio between the peak power and the average power of the transmitted signal. Unlike the average power constraint, the PAPR focuses on limiting the maximum instantaneous power. High PAPR values can cause complications for PAs in transmitters. While these amplifiers achieve maximum power efficiency near saturation, high PAPR signals require significant back-off from saturation to accommodate large peak values without clipping. This forces the amplifier to operate at reduced average power levels relative to its capability, thereby reducing overall power efficiency. By incorporating a PAPR constraint and utilizing clipping techniques, it is possible to maintain signal integrity, enhance PA efficiency, and reduce distortion.

The PAPR of the original time-domain OFDM symbol for the a^{th} antenna can be expressed as

$$\text{PAPR} = \frac{\|\mathbf{x}^a\|_{\infty}^2}{\mathbb{E}[\|\mathbf{x}^a\|_2^2]} = \frac{\max_{n=1, \dots, \ell S} |\mathbf{x}^a[n]|^2}{\mathbb{E}[\|\mathbf{x}^a\|_2^2]}.$$

It is desired to keep the PAPR lower than a threshold PAPR_{max} .

6) *Spectral Shaping Constraint*: The spectral shaping constraint involves techniques that control the OOB power emissions of the transmitted signal to comply with regulatory spectral requirements. MIMO-OFDM systems can exhibit significant OOB power leakage due to the spectral characteristics of the subcarrier waveforms, which can extend beyond the allocated bandwidth. This leakage can interfere with adjacent channels and violate spectral constraints, necessitating the use of spectral shaping techniques. These techniques produce smoother spectral transitions at the edges of the occupied bandwidth, thereby reducing OOB emissions below mandated levels while improving spectral efficiency.

Spectral shaping is accomplished by selecting a precoder that enforces nulling at specifically chosen frequencies, such that $X^a(f_j) = 0$ for each f_j in the set $\{f_1, \dots, f_G\}$. Following the approach in [15], these frequencies are strategically positioned close to each other at the edges of adjacent frequency bands or interference regions. The positioning of closely-spaced frequencies has been shown to significantly improve spectral suppression, effectively creating a discrete approximation to continuous spectral mask constraints while providing the flexibility to adapt to time-varying interference scenarios. To implement constraints at these G frequencies, G linear equations are applied, represented by $\mathbf{A} \mathbf{g}^a = \mathbf{0}$ at antenna a for fully-digital systems and by $\mathbf{A} \mathbf{w}^a = \mathbf{0}$ for hybrid systems. The matrix $\mathbf{A} \in \mathbb{C}^{G \times S}$ is defined as $\mathbf{A} = \{\{o^s(f_j)\}_{s \in \mathcal{S}}\}_{j=1}^G$. Geometrically, this criterion dictates that we optimize the precoders \mathbf{V}_k^s such that \mathbf{w}^a resides in the nullspace of \mathbf{A} , i.e., $\{\mathbf{w}^a \in \mathbb{C}^{S \times 1} | \mathbf{A} \mathbf{w}^a = \mathbf{0}\}$. Such \mathbf{w}^a characterizes precoded OFDM symbols at each antenna, whose Fourier transforms exhibit zeros at the frequency set $\{f_1, \dots, f_G\}$.

This constraint can result in interference reduction instead of complete mitigation as when transmitted symbols are random, nullification constraints cannot be imposed directly on every symbol realization with fixed precoders. Thus, we will show that spectral notching is transformed to mask-compliant

constraints for the probabilistic case. This mask complies with regulatory spectral mask requirements, e.g., 3GPP NR ACLR specifications and unwanted emissions limits [18].

III. PROBLEM FORMULATION

A. Sum-Rate Maximization

The goal in this paper is to maximize the sum-rate of users across all subcarriers when each user receives data on all subcarriers. The sum-rate is $\sum_{k=1}^K \sum_{s \in \mathcal{S}} R_k^s$ where R_k^s is the achievable rate of user k on subcarrier s . The rate calculation assumes that users have perfect channel state information (CSI) and treat interference from other users as independent additive noise, which is a standard assumption in MU-MIMO systems that enables tractable analysis while providing reasonable approximations for practical interference-limited scenarios. Under these assumptions, R_k^s is calculated as follows [4], [28]:

$$R_k^s = \log_2 \left| \mathbf{I}_{n_k} + \mathbf{U}_k^{s^H} \mathbf{U}_{\text{RF},k}^H \mathbf{H}_k^s \mathbf{V}_{\text{RF}} \mathbf{V}_k^s \right. \\ \left. \times \mathbf{V}_k^{s^H} \mathbf{V}_{\text{RF}}^H \mathbf{H}_k^{s^H} \mathbf{U}_{\text{RF},k} \mathbf{U}_k^s \mathbf{J}_k^{s^{-1}} \right|,$$

where

$$\mathbf{J}_k^s = \sum_{j=1, j \neq k}^K \mathbf{U}_k^{s^H} \mathbf{U}_{\text{RF},k}^H \mathbf{H}_k^s \mathbf{V}_{\text{RF}} \mathbf{V}_j^s \mathbf{V}_j^{s^H} \mathbf{V}_{\text{RF}}^H \mathbf{H}_k^{s^H} \mathbf{U}_{\text{RF},k} \mathbf{U}_k^s \\ + \sigma_{\text{noise},k}^{s^2} \mathbf{U}_k^{s^H} \mathbf{U}_{\text{RF},k}^H \mathbf{U}_{\text{RF},k} \mathbf{U}_k^s.$$

The achievable rate is computed using the above matrix formulation where \mathbf{J}_k^s represents the interference-plus-noise covariance matrix that accounts for MU interference and noise contributions in the MIMO system.

We formulate the joint hybrid precoding problem to maximize the user sum-rate, subject to transmit power budget, PAPR, clipping, and spectral shaping constraints as follows:

$$\max_{\{\{\mathbf{V}_k^s\}_{k=1}^K, \mathbf{V}_{\text{RF}}, \{\mathbf{x}^a\}_{a=1}^{N_t}\}_{s \in \mathcal{S}}} \sum_{k=1}^K \sum_{s \in \mathcal{S}} R_k^s \quad (5a)$$

$$\text{subject to: } \sum_{k=1}^K \|\mathbf{V}_{\text{RF}} \mathbf{V}_k^s\|_F^2 \leq P^s, \quad \forall s, \quad (5b)$$

$$\frac{\|\mathbf{x}^a\|_\infty^2}{\mathbb{E}[\|\mathbf{x}^a\|_2^2]} \leq \text{PAPR}_{\max}, \quad \forall a, \quad (5c)$$

$$\|\mathbf{x}^a\|_\infty \leq \chi, \quad \forall a, \quad (5d)$$

$$\mathbf{A} \mathbf{w}^a = \mathbf{0}, \quad \forall a, \quad (5e)$$

$$\mathbf{x}^a = \mathbf{F}^{-1} \mathbf{w}^a \quad \forall a. \quad (5f)$$

This paper leverages the well-established WMMSE approach [21] to maximize the sum-rate. The WMMSE method iteratively optimizes each variable while holding others constant. We note that the transmitted symbol vectors are treated as random complex variables. This inherent randomness poses a challenge in enforcing the constraints deterministically for every possible symbol vector. To address this challenge, we need to consider the constraints from a probabilistic perspective. This ensures that the constraints are met with a high degree of confidence across all possible symbol vector realizations. Therefore, we translate constraints (5c), (5d), and (5e) into their probabilistic constraints in the following section.

B. Reformulation of Constraints

In this section, we analyze the probabilistic perspective of deterministic constraints using the following propositions. These propositions provide insights into the probabilistic bounds on the PAPR, clipping, and the spectral shaping constraints.

Proposition 1. *The probability of the PAPR constraint being satisfied for partially-connected hybrid systems grows with increasing the oversampling factor ℓ .*

Proof. The proof is given in Appendix A. \blacksquare

Proposition 2. *To avoid the signal being clipped with probability of $1 - \epsilon$, when partially-connected hybrid precoding is utilized, the following inequality must hold:*

$$\sqrt{-2 \ln(\epsilon) \left(\sum_{k=1}^K \sum_{s \in \mathcal{S}} \|\mathbf{V}_k^s[m, :] \|^2_2 \right)} \leq \chi, \quad (6)$$

for each RF chain m .

Proof. The proof is given in Appendix B. \blacksquare

The following proposition presents the probabilistic bound on the constraint $\mathbf{A} \mathbf{w}^a = \mathbf{0}$, which serves to minimize OOB emissions in our optimization problem.

Proposition 3. *Let $\mathbf{L}[i, j]$ represent the $(i, j)^{\text{th}}$ element of the matrix $\mathbf{L} = \mathbf{A}^H \mathbf{A}$. If a partially-connected hybrid precoding is utilized, the following constraint ensures that the probability of the squared norm of the residual of $\mathbf{A} \mathbf{w}^a = \mathbf{0}$ being less than ϵ_1 is at least $1 - \epsilon_2$:*

$$\sqrt{\sum_{s \in \mathcal{S}} \mathbf{L}[s, s] \left(\sum_{k=1}^K (\|\mathbf{V}_k^s[m, :] \|^2_2) \right)} \leq \epsilon_1 \sqrt{\epsilon_2}, \quad \forall m. \quad (7)$$

Proof. The proof is given in Appendix C. \blacksquare

IV. THE PROPOSED WMMSE-BASED ALGORITHM

In this section, we develop a novel algorithm based on the WMMSE approach that uses the relationship between the total sum-rate and the mean-square error (MSE). In the WMMSE-based approach, a weighted MSE is minimized with respect to the aforementioned blocks of variables, rather than maximizing (5a). First, we compute the MSE matrix of the estimated signal for user k on subcarrier s as

$$\mathbf{E}_k^s = \mathbb{E}_{\omega, \mathbf{n}} [(\hat{\omega}_k^s - \omega_k^s)(\hat{\omega}_k^s - \omega_k^s)^H] \\ = (\mathbf{I}_{n_k} - \mathbf{U}_k^{s^H} \mathbf{U}_{\text{RF},k}^H \mathbf{H}_k^s \mathbf{V}_{\text{RF}} \mathbf{V}_k^s) \\ (\mathbf{I}_{n_k} - \mathbf{U}_k^{s^H} \mathbf{U}_{\text{RF},k}^H \mathbf{H}_k^s \mathbf{V}_{\text{RF}} \mathbf{V}_k^s)^H \\ + \mathbf{U}_k^{s^H} \mathbf{U}_{\text{RF},k}^H \left(\sum_{j=1, j \neq k}^K \mathbf{H}_k^s \mathbf{V}_{\text{RF}} \mathbf{V}_j^s \mathbf{V}_j^{s^H} \mathbf{V}_{\text{RF}}^H \mathbf{H}_k^{s^H} \right) \mathbf{U}_{\text{RF},k} \mathbf{U}_k^s \\ + \sigma_{\text{noise},k}^{s^2} \mathbf{U}_k^{s^H} \mathbf{U}_{\text{RF},k}^H \mathbf{U}_{\text{RF},k} \mathbf{U}_k^s. \quad (8)$$

The expectation is taken with respect to $\{\omega_k^s\}_{k=1}^K$ and $\{\mathbf{n}_k^s\}_{k=1}^K$. In deriving this expectation, we utilized the properties $\mathbb{E}[\omega_k^s \omega_k^{s^H}] = \mathbf{I}_{n_k}$ and $\mathbb{E}[\omega_k^s \omega_l^{s^H}] = \mathbf{0}_{n_k}$ for $l \neq k$. Following the WMMSE approach [21], we introduce a positive

semi-definite (PSD) weight matrix \mathbf{W}_k^s applied to \mathbf{E}_k^s . This leads to the formulation of an alternative problem to (5):

$$\begin{aligned} \min_{\{\mathbf{U}_{\text{RF},k}, \{\mathbf{V}_{\text{RF}}, \mathbf{U}_k^s, \mathbf{V}_k^s, \mathbf{W}_k^s \succeq \mathbf{0}\}_{s \in \mathcal{S}}\}_{k=1}^K} & \sum_{k=1}^K \sum_{s \in \mathcal{S}} \text{tr}(\mathbf{W}_k^s \mathbf{E}_k^s) - \log(|\mathbf{W}_k^s|) \\ \text{s.t.} & (5b) - (5f). \end{aligned} \quad (9)$$

To solve (9), we employ a BCD approach. This method involves alternately minimizing (9) with respect to different variable blocks until convergence is achieved for all blocks.

A. The Subproblem with Respect to \mathbf{U}_k^s

The problem with respect to \mathbf{U}_k^s is unconstrained. The optimal solution for \mathbf{U}_k^s is determined by the first order optimality condition. Hence, each \mathbf{U}_k^s iterate is updated as

$$\begin{aligned} \mathbf{U}_k^s = & \left(\mathbf{U}_{\text{RF},k}^H \left(\mathbf{H}_k^s \mathbf{V}_{\text{RF}} \left(\sum_{j=1}^K \mathbf{V}_j^s \mathbf{V}_j^{s^H} \right) \mathbf{V}_{\text{RF}}^H \mathbf{H}_k^{s^H} + \sigma_{\text{noise},k}^s \mathbf{I}_{N_r} \right) \right. \\ & \times \left. \mathbf{U}_{\text{RF},k} \right)^{-1} \mathbf{U}_{\text{RF},k}^H \mathbf{H}_k^s \mathbf{V}_{\text{RF}} \mathbf{V}_k^s. \end{aligned} \quad (10)$$

B. The Subproblem with Respect to \mathbf{W}_k^s

We substitute (10) into (8) and obtain the expected MSE as

$$\mathbf{E}_k^s = \mathbf{I}_{n_k} - \mathbf{U}_k^{s^H} \mathbf{U}_{\text{RF},k}^H \mathbf{H}_k^s \mathbf{V}_{\text{RF}} \mathbf{V}_k^s.$$

Substituting \mathbf{E}_k^s into (9), one can obtain \mathbf{W}_k^s from the first order optimality condition as $\mathbf{W}_k^s = (\mathbf{E}_k^s)^{-1}$.

C. The Subproblem with Respect to \mathbf{V}_k^s

As shown in Appendix A, the PAPR can be driven to a desired level by oversampling the signal, regardless of the precoding matrices used. Accordingly, we omit this constraint and assume that the oversampling factor has already been set to an appropriate value.

Let us investigate the maximum power constraint (2). This constraint can be simplified as follows:

$$\sum_{k=1}^K \text{tr}(\mathbf{V}_k^{s^H} \mathbf{V}_{\text{RF}}^H \mathbf{V}_{\text{RF}} \mathbf{V}_k^s) = \sum_{k=1}^K \frac{N_t}{N_{\text{RF}}} \text{tr}(\mathbf{V}_k^{s^H} \mathbf{V}_k^s) \leq P^s,$$

where the above equality holds due to the fact that for partially-connected architecture, $\mathbf{V}_{\text{RF}}^H \mathbf{V}_{\text{RF}} = \frac{N_t}{N_{\text{RF}}} \mathbf{I}_{N_{\text{RF}}}$ [1, Lemma 1].

The problem in (9) is quadratic and convex with respect to \mathbf{V}_k^s . We note that we have multiple constraints for the digital precoders as given in (2), (6), and (7). This makes the problem difficult to solve. To alleviate the complexity of solving the problem, we decompose the problem and decouple constraints using the ADMM approach. Then, instead of solving one big problem, a sequence of smaller problems, each with one constraint, is solved. We copy the precoding variables as $\mathbf{V}_k^s = \mathbf{R}_k^s = \mathbf{Z}_k^s$. We associate Lagrange multipliers $\Lambda_{1,k}^s$ and $\Lambda_{2,k}^s$ to the above equalities and write the augmented Lagrangian as

$$\mathcal{L}(\mathbf{V}_k^s, \mathbf{R}_k^s, \mathbf{Z}_k^s) = \sum_{k=1}^K \sum_{s \in \mathcal{S}} \left[\text{tr}(\mathbf{W}_k^s \mathbf{E}_k^s) \right.$$

$$\begin{aligned} & + \Re(\text{tr}(\Lambda_{1,k}^{s^H} (\mathbf{V}_k^s - \mathbf{R}_k^s))) + \frac{\rho}{2} \|\mathbf{V}_k^s - \mathbf{R}_k^s\|_F^2 \\ & + \Re(\text{tr}(\Lambda_{2,k}^{s^H} (\mathbf{R}_k^s - \mathbf{Z}_k^s))) + \frac{\rho}{2} \|\mathbf{R}_k^s - \mathbf{Z}_k^s\|_F^2 \end{aligned} \quad (11)$$

where $\Re(\cdot)$ represents the real part. In the above equality, ρ is the penalty parameter. There is one maximum power constraint per subcarrier. The subproblem with respect to \mathbf{V}_k^s is

$$\begin{aligned} \min_{\mathbf{V}_k^s} & \sum_{k=1}^K \sum_{s \in \mathcal{S}} \text{tr}(\mathbf{W}_k^s \mathbf{E}_k^s) + \Re(\text{tr}(\Lambda_{1,k}^{s^H} (\mathbf{V}_k^s - \mathbf{R}_k^s))) \\ & + \sum_{k=1}^K \sum_{s \in \mathcal{S}} \frac{\rho}{2} \|\mathbf{V}_k^s - \mathbf{R}_k^s\|_F^2 \\ \text{s.t.} & \sum_{k=1}^K \frac{N_t}{N_{\text{RF}}} \text{tr}(\mathbf{V}_k^{s^H} \mathbf{V}_k^s) \leq P^s. \end{aligned} \quad (12)$$

Moreover, the subproblem with respect to \mathbf{R}_k^s is

$$\begin{aligned} \min_{\mathbf{R}_k^s} & \sum_{k=1}^K \sum_{s \in \mathcal{S}} \Re(\text{tr}(\Lambda_{1,k}^{s^H} (\mathbf{V}_k^s - \mathbf{R}_k^s))) + \frac{\rho}{2} \|\mathbf{V}_k^s - \mathbf{R}_k^s\|_F^2 \\ & + \sum_{k=1}^K \sum_{s \in \mathcal{S}} \Re(\text{tr}(\Lambda_{2,k}^{s^H} (\mathbf{R}_k^s - \mathbf{Z}_k^s))) + \frac{\rho}{2} \|\mathbf{R}_k^s - \mathbf{Z}_k^s\|_F^2 \\ \text{s.t.} & \sqrt{\sum_{s \in \mathcal{S}} \mathbf{L}[s, s] \sum_{k=1}^K \|\mathbf{R}_k^s[m, :]\|_2^2} \leq \sqrt{\epsilon'}, \quad \forall m. \end{aligned}$$

Finally, the subproblem with respect to \mathbf{Z}_k^s is

$$\begin{aligned} \min_{\mathbf{Z}_k^s} & \sum_{k=1}^K \sum_{s \in \mathcal{S}} \Re(\text{tr}(\Lambda_{2,k}^{s^H} (\mathbf{R}_k^s - \mathbf{Z}_k^s))) + \frac{\rho}{2} \|\mathbf{R}_k^s - \mathbf{Z}_k^s\|_F^2 \\ \text{s.t.} & \sqrt{-2 \ln(\epsilon) \left(\sum_{k=1}^K \sum_{s \in \mathcal{S}} \|\mathbf{Z}_k^s[m, :]\|_2^2 \right)} \leq \chi, \quad \forall m. \end{aligned}$$

1) *The Solution for \mathbf{V}_k^s :* After dualizing the power budget constraint, we express the augmented Lagrangian as follows:

$$\begin{aligned} \mathcal{L}(\mathbf{V}^s, \mathbf{R}^s, \Lambda_1^s) = & \sum_{k=1}^K \sum_{s \in \mathcal{S}} \text{tr}(\mathbf{W}_k^s \mathbf{E}_k^s) \\ & + \sum_{k=1}^K \sum_{s \in \mathcal{S}} \Re(\text{tr}(\Lambda_{1,k}^{s^H} (\mathbf{V}_k^s - \mathbf{R}_k^s))) + \sum_{k=1}^K \sum_{s \in \mathcal{S}} \frac{\rho}{2} \|\mathbf{V}_k^s - \mathbf{R}_k^s\|_F^2 \\ & + \sum_{s \in \mathcal{S}} \vartheta^s \left(\sum_{k=1}^K \frac{N_t}{N_{\text{RF}}} \text{tr}(\mathbf{V}_k^{s^H} \mathbf{V}_k^s) - P^s \right). \end{aligned} \quad (15)$$

We have the following KKT conditions:

$$\mathbf{V}_k^s = \left(\sum_{j=1}^K \mathbf{V}_{\text{RF}}^H \mathbf{H}_j^{s^H} \mathbf{U}_{\text{RF},j} \mathbf{U}_j^s \mathbf{W}_j^s \mathbf{U}_j^{s^H} \mathbf{U}_{\text{RF},j}^H \mathbf{H}_j^s \mathbf{V}_{\text{RF}} \right) \quad (16a)$$

$$\begin{aligned} & + \left(\rho/2 + \frac{\vartheta^s N_t}{N_{\text{RF}}} \right)^{-1} \\ & \times \left(\frac{\rho \mathbf{R}_k^s - \Lambda_{1,k}^s}{2} + \mathbf{V}_{\text{RF}}^H \mathbf{H}_k^{s^H} \mathbf{U}_{k,\text{RF}} \mathbf{U}_k^s \mathbf{W}_k^s \right), \\ & \sum_{k=1}^K \frac{N_t}{N_{\text{RF}}} \text{tr}(\mathbf{V}_k^{s^H} \mathbf{V}_k^s) \leq P^s, \end{aligned} \quad (16b)$$

$$\vartheta^s \left(\sum_{k=1}^K \frac{N_t}{N_{\text{RF}}} \text{tr}(\mathbf{V}_k^{s^H} \mathbf{V}_k^s) - P^s \right) = 0, \vartheta^s \geq 0. \quad (16c)$$

The optimal ϑ^s can be obtained through a bisection-search over the positive orthant (where \mathbf{V}_k^s derived from (16a)) to satisfy $\sum_{k=1}^K \frac{N_t}{N_{\text{RF}}} \text{tr}(\mathbf{V}_k^{s^H} \mathbf{V}_k^s) = P^s$. If no positive ϑ^s satisfies this condition, we can set $\vartheta^s = 0$ and compute \mathbf{V}_k^s from (16a).

Since the subproblem (12) is convex, the global optimal solution can be obtained with the KKT conditions [29, Sec. 5.5.3].

2) *The Solution for \mathbf{R}_k^s :* Due to the strong convexity of (11), the solution to \mathbf{R}_k^s can be found in closed-form, followed by a projection. Setting the derivative of (11) with respect to \mathbf{R}_k^s to zero, the minimizer of (11) is obtained as follows:

$$\tilde{\mathbf{R}}_k^s = \frac{1}{2} \left(\mathbf{V}_k^s + \frac{\Lambda_{1,k}^s}{\rho} + \mathbf{Z}_k^s - \frac{\Lambda_{2,k}^s}{\rho} \right). \quad (17)$$

To project the above solution to the reformulated spectral shaping constraint, we use the following per RF chain form:

$$\mathbf{R}_k^s[m, :] = \begin{cases} \sqrt{\epsilon'} \tilde{\mathbf{R}}_k^s[m, :] / \sqrt{\sum_{s \in \mathcal{S}} \mathbf{L}[s, s] \sum_{k=1}^K \|\tilde{\mathbf{R}}_k^s[m, :]\|_2^2}, & \text{if } \sqrt{\sum_{s \in \mathcal{S}} \mathbf{L}[s, s] \sum_{k=1}^K \|\tilde{\mathbf{R}}_k^s[m, :]\|_2^2} > \sqrt{\epsilon'}, \\ \tilde{\mathbf{R}}_k^s[m, :], & \text{o.w.} \end{cases} \quad (18)$$

3) *The Solution for \mathbf{Z}_k^s :* The Lagrangian minimization with respect to \mathbf{Z}_k^s is strongly convex. The minimizer of (11) can be obtained by setting the derivative with respect to \mathbf{Z}_k^s to zero as follows:

$$\tilde{\mathbf{Z}}_k^s = \mathbf{R}_k^s + \frac{\Lambda_{2,k}^s}{\rho}. \quad (19)$$

To project the above solution to (6), we use the following per RF chain equation:

$$\mathbf{Z}_k^s = \begin{cases} \frac{\chi}{\sqrt{-2 \ln(\epsilon)}} \tilde{\mathbf{Z}}_k^s[m, :] / \sqrt{\sum_{k=1}^K \sum_{s \in \mathcal{S}} \|\tilde{\mathbf{Z}}_k^s[m, :]\|_2^2}, & \text{if } \sqrt{\sum_{k=1}^K \sum_{s \in \mathcal{S}} \|\tilde{\mathbf{Z}}_k^s[m, :]\|_2^2} > \frac{\chi}{\sqrt{-2 \ln(\epsilon)}}, \\ \tilde{\mathbf{Z}}_k^s[m, :], & \text{o.w.} \end{cases} \quad (20)$$

4) *The Proposed ADMM Approach:* In the proposed ADMM algorithm, the three primal blocks are updated sequentially with the Gauss-Seidel rule as described in Algorithm 1. Once primal variable blocks are updated, dual blocks are updated in the $\tau + 1^{\text{th}}$ iteration using the following equations:

$$\Lambda_{1,k}^{s,\tau+1} = \Lambda_{1,k}^{s,\tau} + \rho(\mathbf{V}_k^{s,\tau+1} - \mathbf{R}_k^{s,\tau+1}), \quad (21)$$

$$\Lambda_{2,k}^{s,\tau+1} = \Lambda_{2,k}^{s,\tau} + \rho(\mathbf{R}_k^{s,\tau+1} - \mathbf{Z}_k^{s,\tau+1}). \quad (22)$$

We alternatively update primal and dual variable blocks until all blocks converge. To accelerate the convergence of the ADMM algorithm, one can use increasing penalty values with the iteration number as $\rho^{\tau+1} = q^{\tau} \rho^{\tau}$, $q^{\tau} > 1$, based on the primal and dual residuals detailed in [30, eq. (3.13)]. Since the subproblem with respect to \mathbf{V}_k^s (subject to (5b), (6), and (7)) is convex, and also subproblems in \mathbf{R}_k^s and \mathbf{Z}_k^s are solved to global optimality, the proposed ADMM converges to the global optimal solution [30].

Algorithm 1: The Proposed ADMM Algorithm

Input: $\mathbf{V}_k^{s,0}, \mathbf{R}_k^{s,0}, \mathbf{Z}_k^{s,0}, \Lambda_1^{s,0}, \Lambda_2^{s,0}$;

Initialize $\tau = 0$;

while $\mathbf{V}_k^{s,\tau}$ not converged **do**

 Update $\mathbf{V}_k^{s,\tau+1}$ using (16) via $\mathbf{R}_k^{s,\tau}$ and $\Lambda_{1,k}^{s,\tau}$;

 Update $\mathbf{R}_k^{s,\tau+1}$ using (17)-(18) via $\mathbf{V}_k^{s,\tau+1}, \mathbf{Z}_k^{s,\tau}, \Lambda_{1,k}^{s,\tau}$ and $\Lambda_{2,k}^{s,\tau}$;

 Update $\mathbf{Z}_k^{s,\tau+1}$ using (19)-(20) via $\mathbf{R}_k^{s,\tau+1}$ and $\Lambda_{2,k}^{s,\tau}$;

 Update the dual variable blocks via (21)-(22) ;

$\tau \leftarrow \tau + 1$;

Output: $\mathbf{V}_k^{s,\tau}$;

D. The Subproblem with Respect to \mathbf{V}_{RF}

PSs in the RF precoding stage of a hybrid MIMO-OFDM system adjust signal phases to create desired beam patterns. PSs are identical across all subcarriers for each antenna, given that RF beamforming occurs before the OFDM modulation. Inefficient PS adjustments change the effective channel by altering the phase relationship between transmitted signals and precoding vectors, leading to precoding gain loss as the intended precoding directions are not perfectly achieved.

We simplify the optimization of phase shifts by PSs as follows. We note that $\sum_{j=1}^K \mathbf{V}_j^s \mathbf{V}_j^{s^H}$ is a positive semi-definite (PSD) matrix since $\mathbf{V}_j^s \mathbf{V}_j^{s^H}$ is a PSD matrix and the sum of PSD matrices is a PSD matrix. Let Θ^s represent the square root of $\sum_{j=1}^K \mathbf{V}_j^s \mathbf{V}_j^{s^H}$. Hence, we have $\Theta^s \Theta^{s^H} = \sum_{j=1}^K \mathbf{V}_j^s \mathbf{V}_j^{s^H}$. Let \mathbf{v}_{PS} represent a vector where the i^{th} element denotes the phase shift applied to the i^{th} antenna. It is straightforward to show that the following equality holds:

$$\mathbf{V}_{\text{RF}} \Theta^s \Theta^{s^H} \mathbf{V}_{\text{RF}}^H = \text{diag}(\mathbf{v}_{\text{PS}}) \mathbf{\Gamma}^s \text{diag}(\mathbf{v}_{\text{PS}})^H,$$

with $\mathbf{\Gamma}^s[i, j] = \Theta^s[m_1, :] \Theta^{s^H}[m_2, :]$, where the i^{th} antenna is connected to the m_1^{th} RF-chain and the j^{th} antenna is connected to the m_2^{th} RF-chain. We simplify the expected MSE and keep those terms that contain \mathbf{V}_{RF} as follows:

$$\begin{aligned} \mathbf{E}_k^{s, \text{simplified}} &= -\mathbf{U}_k^{s^H} \mathbf{U}_{\text{RF},k}^H \mathbf{H}_k^s \mathbf{V}_{\text{RF}} \mathbf{V}_k^s \\ &\quad - (\mathbf{U}_k^{s^H} \mathbf{U}_{\text{RF},k}^H \mathbf{H}_k^s \mathbf{V}_{\text{RF}} \mathbf{V}_k^s)^H \\ &\quad + \mathbf{U}_k^{s^H} \mathbf{U}_{\text{RF},k}^H \left(\sum_{j=1}^K \mathbf{H}_k^s \mathbf{V}_{\text{RF}} \mathbf{V}_j^s \mathbf{V}_j^{s^H} \mathbf{V}_{\text{RF}}^H \mathbf{H}_k^{s^H} \right) \mathbf{U}_{\text{RF},k} \mathbf{U}_k^s \\ &= -\mathbf{U}_k^{s^H} \mathbf{U}_{\text{RF},k}^H \mathbf{H}_k^s \mathbf{V}_{\text{RF}} \mathbf{V}_k^s - (\mathbf{U}_k^{s^H} \mathbf{U}_{\text{RF},k}^H \mathbf{H}_k^s \mathbf{V}_{\text{RF}} \mathbf{V}_k^s)^H \\ &\quad + \mathbf{U}_k^{s^H} \mathbf{U}_{\text{RF},k}^H \left(\mathbf{H}_k^s \text{diag}(\mathbf{v}_{\text{PS}}) \mathbf{\Gamma}^s \text{diag}(\mathbf{v}_{\text{PS}})^H \mathbf{H}_k^{s^H} \right) \mathbf{U}_{\text{RF},k} \mathbf{U}_k^s. \end{aligned}$$

To optimize \mathbf{V}_{RF} , we minimize $\sum_{s \in \mathcal{S}} \sum_{k=1}^K \text{tr}(\mathbf{W}_k^s \mathbf{E}_k^{s, \text{simplified}})$. To simplify the problem, we consider the following equality. For general matrices \mathbf{A} , \mathbf{B} , and \mathbf{C} , we have $\text{tr}(\mathbf{A}^H (\mathbf{B} \odot \mathbf{C})) = \text{vec}(\mathbf{A})^H \text{diag}(\text{vec}(\mathbf{B})) \text{vec}(\mathbf{C})$. Using this equality, we simplify the linear term in the above expression as follows:

$$\sum_{s \in \mathcal{S}} \sum_{k=1}^K \text{tr}(\mathbf{V}_k^s \mathbf{W}_k^s \mathbf{U}_k^{s^H} \mathbf{U}_{\text{RF},k}^H \mathbf{H}_k^s \mathbf{V}_{\text{RF}})$$

$$= \underbrace{\sum_{s \in \mathcal{S}} \sum_{k=1}^K \text{vec}((\mathbf{V}_k^s \mathbf{W}_k^s \mathbf{U}_k^s \mathbf{U}_{\text{RF},k}^H \mathbf{H}_k^s)^H)^H}_{\bar{\mathbf{u}}_{\text{PS}}^H} \bar{\mathbf{v}}_{\text{PS}},$$

where $\bar{\mathbf{v}}_{\text{PS}} \triangleq \text{vec}(\mathbf{V}_{\text{RF}})$. We represent the vector of element indices for which $\text{vec}(\mathbf{V}_{\text{RF}})$ is non-zero by idx . Then, we have $\mathbf{u}_{\text{PS}} = \bar{\mathbf{u}}_{\text{PS}}[\text{idx}]$ and $\mathbf{v}_{\text{PS}} = \bar{\mathbf{v}}_{\text{PS}}[\text{idx}]$. Therefore, we can rewrite the above equation as $\bar{\mathbf{u}}_{\text{PS}}^H \bar{\mathbf{v}}_{\text{PS}}$.

Next, we simplify the quadratic term of \mathbf{V}_{RF} . For a diagonal matrix $\mathbf{\Pi} = \text{diag}(\boldsymbol{\pi})$, we have a useful equality $\text{tr}(\mathbf{\Pi}^H \mathbf{A} \mathbf{\Pi} \mathbf{B}) = \boldsymbol{\pi}^H (\mathbf{A} \odot \mathbf{B}^T) \boldsymbol{\pi}$. We use this equality to apply the following simplification of the quadratic term in \mathbf{v}_{PS} :

$$\begin{aligned} & \sum_{s \in \mathcal{S}} \sum_{k=1}^K \text{tr} \left(\text{diag}(\mathbf{v}_{\text{PS}}^H) (\mathbf{H}_k^{s^H} \mathbf{U}_{\text{RF},k} \mathbf{U}_k^s \mathbf{W}_k^s \mathbf{U}_k^s \mathbf{U}_{\text{RF},k}^H \mathbf{H}_k^s) \text{diag}(\mathbf{v}_{\text{PS}}) \mathbf{\Gamma}^s \right) \\ &= \mathbf{v}_{\text{PS}}^H \underbrace{\left(\sum_{s \in \mathcal{S}} \sum_{k=1}^K ((\mathbf{H}_k^{s^H} \mathbf{U}_{\text{RF},k} \mathbf{U}_k^s \mathbf{W}_k^s \mathbf{U}_k^s \mathbf{U}_{\text{RF},k}^H \mathbf{H}_k^s) \odot \mathbf{\Gamma}^{s^T}) \right)}_{\mathbf{Q}_{\text{PS}}} \mathbf{v}_{\text{PS}}. \end{aligned}$$

Using the above equations, those terms of the simplified weighted MSE that include \mathbf{v}_{PS} can be rewritten as follows:

$$f(\mathbf{v}_{\text{PS}}) = \mathbf{v}_{\text{PS}}^H \mathbf{Q}_{\text{PS}} \mathbf{v}_{\text{PS}} - 2\Re(\mathbf{u}_{\text{PS}}^H \mathbf{v}_{\text{PS}}). \quad (23)$$

Due to the non-convex nature of the unit-magnitude constraints, we propose an element-wise iterative approach that optimizes one variable at a time while keeping others fixed. First, we expand the objective function as $f(\mathbf{v}_{\text{PS}}) = \sum_{i=1}^{N_t} \sum_{j=1}^{N_t} \mathbf{v}_{\text{PS}}^*[i] \mathbf{Q}_{\text{PS}}[i, j] \mathbf{v}_{\text{PS}}[j] - 2 \sum_{j=1}^{N_t} \Re(\mathbf{u}_{\text{PS}}^*[j] \mathbf{v}_{\text{PS}}[j])$. To optimize $\mathbf{v}_{\text{PS}}[a]$, we fix all other elements $\mathbf{v}_{\text{PS}}[j]$ for $j \neq a$ and separate the objective function into terms involving $\mathbf{v}_{\text{PS}}[a]$:

$$\begin{aligned} f(\mathbf{v}_{\text{PS}}) &= \underbrace{\sum_{\substack{i=1, i \neq a \\ j=1, j \neq a}}^{N_t} \mathbf{v}_{\text{PS}}^*[i] \mathbf{Q}_{\text{PS}}[i, j] \mathbf{v}_{\text{PS}}[j] - 2 \sum_{\substack{j=1 \\ j \neq a}}^{N_t} \Re(\mathbf{u}_{\text{PS}}^*[j] \mathbf{v}_{\text{PS}}[j])}_{\text{fixed}} \\ &+ \underbrace{\sum_{\substack{j=1 \\ j \neq a}}^{N_t} \mathbf{v}_{\text{PS}}^*[a] \mathbf{Q}_{\text{PS}}[a, j] \mathbf{v}_{\text{PS}}[j]}_{\text{linear in } \mathbf{v}_{\text{PS}}^*[a]} + \underbrace{\sum_{\substack{i=1 \\ i \neq a}}^{N_t} \mathbf{v}_{\text{PS}}^*[i] \mathbf{Q}_{\text{PS}}[i, a] \mathbf{v}_{\text{PS}}[a]}_{\text{linear in } \mathbf{v}_{\text{PS}}[a]} \\ &+ \underbrace{\mathbf{v}_{\text{PS}}^*[a] \mathbf{Q}_{\text{PS}}[a, a] \mathbf{v}_{\text{PS}}[a]}_{\text{quadratic}} - \underbrace{2\Re(\mathbf{u}_{\text{PS}}^*[a] \mathbf{v}_{\text{PS}}[a])}_{\text{linear}}. \end{aligned}$$

Since \mathbf{Q}_{PS} is Hermitian, we have $\sum_{\substack{i=1 \\ i \neq a}}^{N_t} \mathbf{v}_{\text{PS}}^*[i] \mathbf{Q}_{\text{PS}}[i, a] = \left(\sum_{\substack{j=1 \\ j \neq a}}^{N_t} \mathbf{Q}_{\text{PS}}[a, j] \mathbf{v}_{\text{PS}}[j] \right)^*$, so the objective function is as follows:

$$\begin{aligned} f(\mathbf{v}_{\text{PS}}) &= \text{const} + \mathbf{Q}_{\text{PS}}[a, a] |\mathbf{v}_{\text{PS}}[a]|^2 \\ &+ 2\Re \left(\left(\left(\sum_{\substack{j=1 \\ j \neq a}}^{N_t} \mathbf{Q}_{\text{PS}}[a, j] \mathbf{v}_{\text{PS}}[j] \right)^* - \mathbf{u}_{\text{PS}}^*[a] \right) \mathbf{v}_{\text{PS}}[a] \right). \end{aligned}$$

Since $|\mathbf{v}_{\text{PS}}[a]| = 1$, to minimize the above objective function, we need to minimize the real part of the

product $\left(\left(\sum_{\substack{j=1 \\ j \neq a}}^{N_t} \mathbf{Q}_{\text{PS}}[a, j] \mathbf{v}_{\text{PS}}[j] \right)^* - \mathbf{u}_{\text{PS}}^*[a] \right) \mathbf{v}_{\text{PS}}[a]$. This is achieved when the phase of $\mathbf{v}_{\text{PS}}[a]$ is aligned opposite to the phase of $\left(\sum_{\substack{j=1 \\ j \neq a}}^{N_t} \mathbf{Q}_{\text{PS}}[a, j] \mathbf{v}_{\text{PS}}[j] \right)^* - \mathbf{u}_{\text{PS}}^*[a]$, i.e., 180 degrees apart. Therefore, we have

$$\mathbf{v}_{\text{PS}}[a] = - \frac{\left(\sum_{\substack{j=1 \\ j \neq a}}^{N_t} \mathbf{Q}_{\text{PS}}[a, j] \mathbf{v}_{\text{PS}}[j] \right)^* - \mathbf{u}_{\text{PS}}^*[a]}{\left| \left(\sum_{\substack{j=1 \\ j \neq a}}^{N_t} \mathbf{Q}_{\text{PS}}[a, j] \mathbf{v}_{\text{PS}}[j] \right)^* - \mathbf{u}_{\text{PS}}^*[a] \right|}. \quad (24)$$

We employ a coordinate descent approach where we iteratively update each element $\mathbf{v}_{\text{PS}}[a]$ while keeping all other elements fixed. At iteration τ , when updating element a , we use the most recently updated values from the current iteration for elements $1, \dots, a-1$ and the values from the previous iteration $\tau-1$ for elements $a+1, \dots, N_t$. This coordinate descent procedure is repeated until convergence, ensuring that each element maintains unit magnitude while monotonically decreasing the objective function. Since each element-wise update minimizes the objective function with respect to that variable while keeping others fixed, and the feasible set is compact, the algorithm is guaranteed to converge to a stationary point [31].

PS impairments in mmWave hybrid beamforming systems introduce random phase errors that significantly degrade system performance. These impairments are modeled as complex exponential terms with Gaussian-distributed phase errors, where each PS element experiences independent random phase deviations from its intended value due to hardware tolerances and manufacturing variations [25], [26]. Unlike common phase noise from a shared local oscillator (LO) that affects all antennas equally as a multiplicative factor and preserves beamforming direction, PS phase errors are element-specific and occur each time new digital and RF precoding matrices are calculated and the RF precoding needs to be applied to the hardware. Independent PS errors destroy the intended beamforming pattern by introducing uncorrelated phase deviations at each antenna. These PS phase errors change whenever the beamforming configuration is updated, with each element experiencing independent deviations from its target phase. To analyze the impact of these impairments on the beamforming objective function, we evaluate the expected value of the quadratic form over the random phase error realizations and derive tractable expressions for robust optimization frameworks.

Starting from the given objective function (23), taking the expectation with respect to the phase errors in \mathbf{v}_{PS} results in:

$$\mathbb{E}_{\mathbf{e}_{\text{error}}} [f(\mathbf{v}_{\text{PS}})] = \mathbb{E}_{\mathbf{e}_{\text{error}}} [\mathbf{v}_{\text{PS}}^H \mathbf{Q}_{\text{PS}} \mathbf{v}_{\text{PS}}] - 2\mathbb{E}_{\mathbf{e}_{\text{error}}} [\Re(\mathbf{u}_{\text{PS}}^H \mathbf{v}_{\text{PS}})].$$

Let $\mathbf{v}_{\text{PS}} = \tilde{\mathbf{v}}_{\text{PS}} \odot \mathbf{e}_{\text{error}}$, where $\tilde{\mathbf{v}}_{\text{PS}}$ denotes the vector of intended phase shifts and $\mathbf{e}_{\text{error}} = [e^{i\Delta\theta_1}, e^{i\Delta\theta_2}, \dots, e^{i\Delta\theta_{N_t}}]^T$ with $\Delta\theta_i \sim \mathcal{N}(0, \sigma_e^2)$. For the first term, we obtain

$$\begin{aligned} \mathbb{E}_{\mathbf{e}_{\text{error}}} [\mathbf{v}_{\text{PS}}^H \mathbf{Q}_{\text{PS}} \mathbf{v}_{\text{PS}}] &= \mathbb{E}_{\mathbf{e}_{\text{error}}} [(\tilde{\mathbf{v}}_{\text{PS}} \odot \mathbf{e}_{\text{error}})^H \mathbf{Q}_{\text{PS}} (\tilde{\mathbf{v}}_{\text{PS}} \odot \mathbf{e}_{\text{error}})] \\ &= \sum_{i=1, j=1}^{N_t} \mathbf{Q}_{\text{PS}}[i, j] \tilde{\mathbf{v}}_{\text{PS}}^*[i] \tilde{\mathbf{v}}_{\text{PS}}[j] \mathbb{E}_{\mathbf{e}_{\text{error}}} [e^{-i\Delta\theta_i} e^{i\Delta\theta_j}] \end{aligned}$$

$$= \sum_{i=1, j=1}^{N_t} \mathbf{Q}_{\text{PS}}[i, j] \tilde{\mathbf{v}}_{\text{PS}}^*[i] \tilde{\mathbf{v}}_{\text{PS}}[j] \mathbb{E}_{\mathbf{e}_{\text{error}}} [e^{\iota(\Delta\theta_j - \Delta\theta_i)}].$$

Since $\Delta\theta_i \sim \mathcal{N}(0, \sigma_e^2)$ are independent, using the moment-generating function, we have $\mathbb{E}_{\mathbf{e}_{\text{error}}} [e^{\iota\Delta\theta_j}] = e^{-\sigma_e^2/2}$ and $\mathbb{E}_{\mathbf{e}_{\text{error}}} [e^{\iota(\Delta\theta_j - \Delta\theta_i)}] = 1$ if $i = j$, and $\mathbb{E}_{\mathbf{e}_{\text{error}}} [e^{\iota(\Delta\theta_j - \Delta\theta_i)}] = \mathbb{E}_{\mathbf{e}_{\text{error}}} [e^{\iota\Delta\theta_j}] \mathbb{E}_{\mathbf{e}_{\text{error}}} [e^{-\iota\Delta\theta_i}] = e^{-\sigma_e^2}$ if $i \neq j$. Therefore, we obtain

$$\begin{aligned} \mathbb{E}_{\mathbf{e}_{\text{error}}} [\tilde{\mathbf{v}}_{\text{PS}}^H \mathbf{Q}_{\text{PS}} \tilde{\mathbf{v}}_{\text{PS}}] &= \sum_{i=1}^{N_t} \mathbf{Q}_{\text{PS}}[i, i] |\tilde{\mathbf{v}}_{\text{PS}}[i]|^2 \\ &+ e^{-\sigma_e^2} \sum_{i=1, j=1, i \neq j}^{N_t} \mathbf{Q}_{\text{PS}}[i, j] \tilde{\mathbf{v}}_{\text{PS}}^*[i] \tilde{\mathbf{v}}_{\text{PS}}[j] = \tilde{\mathbf{v}}_{\text{PS}}^H (\mathbf{Q}_{\text{PS}} \odot \mathbf{I}_{N_t}) \tilde{\mathbf{v}}_{\text{PS}} \\ &+ e^{-\sigma_e^2} \tilde{\mathbf{v}}_{\text{PS}}^H (\mathbf{Q}_{\text{PS}} \odot (\mathbf{1}_{N_t} - \mathbf{I}_{N_t})) \tilde{\mathbf{v}}_{\text{PS}}, \end{aligned}$$

where $\mathbf{1}_{N_t}$ is the all-ones matrix and \odot denotes the Hadamard product. The second term is calculated as

$$\mathbb{E}_{\mathbf{e}_{\text{error}}} [\Re(\mathbf{u}_{\text{PS}}^H \tilde{\mathbf{v}}_{\text{PS}})] = \Re(\mathbf{u}_{\text{PS}}^H \tilde{\mathbf{v}}_{\text{PS}} \mathbb{E}[e^{\iota\Delta\theta_i}]) = e^{-\sigma_e^2/2} \Re(\mathbf{u}_{\text{PS}}^H \tilde{\mathbf{v}}_{\text{PS}}).$$

The final simplified expectation becomes

$$\begin{aligned} \mathbb{E}_{\mathbf{e}_{\text{error}}} [f(\mathbf{v}_{\text{PS}})] &= -2e^{-\sigma_e^2/2} \Re(\mathbf{u}_{\text{PS}}^H \tilde{\mathbf{v}}_{\text{PS}}) \\ &+ \tilde{\mathbf{v}}_{\text{PS}}^H \underbrace{[\mathbf{Q}_{\text{PS}} \odot \mathbf{I}_{N_t} + e^{-\sigma_e^2} (\mathbf{Q}_{\text{PS}} \odot (\mathbf{1}_{N_t} - \mathbf{I}_{N_t}))]}_{\tilde{\mathbf{Q}}_{\text{PS}}} \tilde{\mathbf{v}}_{\text{PS}}. \end{aligned}$$

Similar to the analysis given before, the update rule for each phase shift can be obtained as follows:

$$\tilde{\mathbf{v}}_{\text{PS}}[a] = -\frac{\left(\sum_{j=1}^{N_t} \tilde{\mathbf{Q}}_{\text{PS}}[a, j] \tilde{\mathbf{v}}_{\text{PS}}[j] \right) - e^{-\sigma_e^2/2} \mathbf{u}_{\text{PS}}[a]}{\left| \left(\sum_{j=1}^{N_t} \tilde{\mathbf{Q}}_{\text{PS}}[a, j] \tilde{\mathbf{v}}_{\text{PS}}[j] \right)^* - e^{-\sigma_e^2/2} \mathbf{u}_{\text{PS}}^*[a] \right|}.$$

Although it was assumed that the phase error of each PS follows a Gaussian distribution, one can repeat the above analysis for any desired distribution.

E. The Subproblem with Respect to Analog Combining $\mathbf{U}_{\text{RF},k}$

To optimize the analog combiner at user k , we need to minimize the following expression with respect to $\mathbf{U}_{\text{RF},k}$:

$$\begin{aligned} &- \sum_{s \in \mathcal{S}} \text{tr}(\mathbf{W}_k^s \mathbf{U}_k^{s^H} \mathbf{U}_{\text{RF},k}^H \mathbf{H}_k^s \mathbf{V}_{\text{RF}} \mathbf{V}_k^s) \quad (25) \\ &- \sum_{s \in \mathcal{S}} \text{tr}(\mathbf{W}_k^s (\mathbf{U}_k^{s^H} \mathbf{U}_{\text{RF},k}^H \mathbf{H}_k^s \mathbf{V}_{\text{RF}} \mathbf{V}_k^s)^H) + \sum_{s \in \mathcal{S}} \text{tr}(\mathbf{W}_k^s \mathbf{U}_k^{s^H} \\ &\times \mathbf{U}_{\text{RF},k}^H \mathbf{H}_k^s \mathbf{V}_{\text{RF}} \left(\sum_{j=1}^K \mathbf{V}_j^s \mathbf{V}_j^{s^H} \right) \mathbf{V}_{\text{RF}}^H \mathbf{H}_k^{s^H} \mathbf{U}_{\text{RF},k} \mathbf{U}_k^s). \end{aligned}$$

To optimize with respect to the (a, m) -th entry $\mathbf{U}_{\text{RF},k}[a, m]$ of $\mathbf{U}_{\text{RF},k}$, we fix all other entries and decompose the objective function. Using the trace property $\text{tr}(\mathbf{AB}) = \sum_{i,j} \mathbf{A}[i, j] \mathbf{B}[j, i]$, we can rewrite each term in the objective function. For the (a, m) -th entry of $\mathbf{U}_{\text{RF},k}$, we extract terms as follows:

$$\sum_{s \in \mathcal{S}} \text{tr}(\mathbf{U}_{\text{RF},k}^H \mathbf{H}_k^s \mathbf{V}_{\text{RF}} \mathbf{V}_k^s \mathbf{W}_k^s \mathbf{U}_k^{s^H})$$

$$= \sum_{s \in \mathcal{S}} \sum_{i, j, \ell} \mathbf{U}_{\text{RF},k}^*[j, i] [\mathbf{H}_k^s \mathbf{V}_{\text{RF}} \mathbf{V}_k^s \mathbf{W}_k^s]_{j, \ell} \mathbf{U}_k^{s^*}[i, \ell].$$

To find terms involving $\mathbf{U}_{\text{RF},k}[a, m]$, we set $j = a$ and $i = m$ in the above expression. We have the following simplifications:

$$\begin{aligned} &\sum_{s \in \mathcal{S}} \mathbf{U}_{\text{RF},k}^*[a, m] \sum_{\ell} [\mathbf{H}_k^s \mathbf{V}_{\text{RF}} \mathbf{V}_k^s \mathbf{W}_k^s]_{a, \ell} \mathbf{U}_k^{s^*}[m, \ell] \\ &= \mathbf{U}_{\text{RF},k}^*[a, m] \underbrace{\sum_{s \in \mathcal{S}} \sum_{\ell} [\mathbf{H}_k^s \mathbf{V}_{\text{RF}} \mathbf{V}_k^s \mathbf{W}_k^s]_{a, \ell} \mathbf{U}_k^{s^*}[m, \ell]}_{\delta_{am}^1}. \end{aligned}$$

Therefore, the contribution to the objective function from this term is $\mathbf{U}_{\text{RF},k}^*[a, m] \delta_{am}^1$. We simplify the term of (25) that is quadratic in $\mathbf{U}_{\text{RF},k}$ as

$$\begin{aligned} &\sum_{s \in \mathcal{S}} \text{tr} \left(\mathbf{W}_k^s \mathbf{U}_k^{s^H} \mathbf{U}_{\text{RF},k}^H \mathbf{H}_k^s \mathbf{V}_{\text{RF}} \left(\sum_{j=1}^K \mathbf{V}_j^s \mathbf{V}_j^{s^H} \right) \mathbf{V}_{\text{RF}}^H \mathbf{H}_k^{s^H} \mathbf{U}_{\text{RF},k} \right. \\ &\times \mathbf{U}_k^s \left. \right) = \sum_{s \in \mathcal{S}} \sum_{i, j, \ell, p, q, r} \mathbf{W}_k^s[i, j] \mathbf{U}_k^{s^*}[\ell, j] \mathbf{U}_{\text{RF},k}^*[p, \ell] \mathbf{O}_k^s[p, q] \\ &\times \mathbf{U}_{\text{RF},k}[q, r] \mathbf{U}_k^s[r, i], \end{aligned} \quad (26)$$

where we define $\mathbf{O}_k^s \triangleq \mathbf{H}_k^s \mathbf{V}_{\text{RF}} \left(\sum_{j=1}^K \mathbf{V}_j^s \mathbf{V}_j^{s^H} \right) \mathbf{V}_{\text{RF}}^H \mathbf{H}_k^{s^H}$.

To extract the quadratic coefficient for $\mathbf{U}_{\text{RF},k}[a, m]$, we identify terms where this entry appears twice: once as $\mathbf{U}_{\text{RF},k}^*[p, \ell]$ and once as $\mathbf{U}_{\text{RF},k}[q, r]$. This occurs when $(p, \ell) = (a, m)$ and $(q, r) = (a, m)$, simultaneously. To analyze the dependence on $\mathbf{U}_{\text{RF},k}[a, m]$, we partition the terms based on how this element appears in (26). There are three cases where $\mathbf{U}_{\text{RF},k}[a, m]$ appears in (26):

- 1) Linear terms where $\mathbf{U}_{\text{RF},k}[p, \ell] = \mathbf{U}_{\text{RF},k}[a, m]$ but $\mathbf{U}_{\text{RF},k}[q, r] \neq \mathbf{U}_{\text{RF},k}[a, m]$:

$$\begin{aligned} &\mathbf{U}_{\text{RF},k}^*[a, m] \sum_{s \in \mathcal{S}} \sum_{i, j} \sum_{\substack{q, r \\ (q, r) \neq (a, m)}} \mathbf{W}_k^s[i, j] \mathbf{U}_k^{s^*}[m, j] \\ &\times \underbrace{\mathbf{O}_k^s[a, q] \mathbf{U}_{\text{RF},k}[q, r] \mathbf{U}_k^s[r, i]}_{\delta_{am}^2}. \end{aligned}$$

- 2) Linear terms where $\mathbf{U}_{\text{RF},k}[q, r] = \mathbf{U}_{\text{RF},k}[a, m]$ but $\mathbf{U}_{\text{RF},k}[p, \ell] \neq \mathbf{U}_{\text{RF},k}[a, m]$:

$$\begin{aligned} &\mathbf{U}_{\text{RF},k}[a, m] \sum_{s \in \mathcal{S}} \sum_{i, j} \sum_{\substack{\ell, p \\ (p, \ell) \neq (a, m)}} \mathbf{W}_k^s[i, j] \mathbf{U}_k^{s^*}[\ell, j] \mathbf{U}_{\text{RF},k}^*[p, \ell] \\ &\times \underbrace{\mathbf{O}_k^s[p, a] \mathbf{U}_k^s[m, i]}_{\delta_{am}^3}. \end{aligned}$$

- 3) Quadratic terms where both $\mathbf{U}_{\text{RF},k}[p, \ell] = \mathbf{U}_{\text{RF},k}[a, m]$ and $\mathbf{U}_{\text{RF},k}[q, r] = \mathbf{U}_{\text{RF},k}[a, m]$:

$$|\mathbf{U}_{\text{RF},k}[a, m]|^2 \sum_{s \in \mathcal{S}} \sum_{i, j} \mathbf{W}_k^s[i, j] \mathbf{U}_k^{s^*}[m, j] \mathbf{O}_k^s[a, a] \mathbf{U}_k^s[m, i].$$

Since \mathbf{W}_k^s and \mathbf{O}_k^s are PSD matrices, one can observe that $\delta_{am}^3 = \delta_{am}^{2*}$. Collecting all terms in one place, we have

$$- \mathbf{U}_{\text{RF},k}^*[a, m] \delta_{am}^1 - \mathbf{U}_{\text{RF},k}[a, m] \delta_{am}^{1*} + \mathbf{U}_{\text{RF},k}^*[a, m] \delta_{am}^2$$

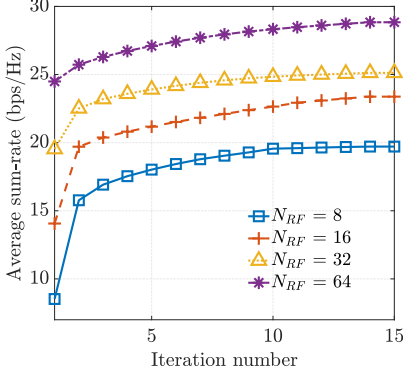


Fig. 1: The convergence of the proposed BCD approach.

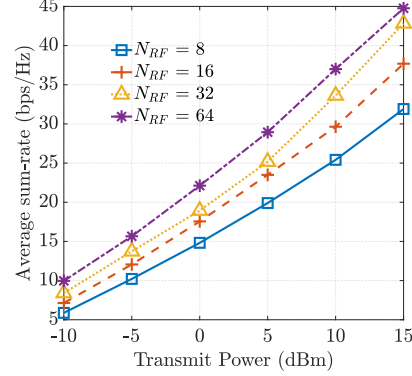


Fig. 2: Average per-subcarrier achievable sum-rate with different transmitter RF chain numbers and $S = 32$.

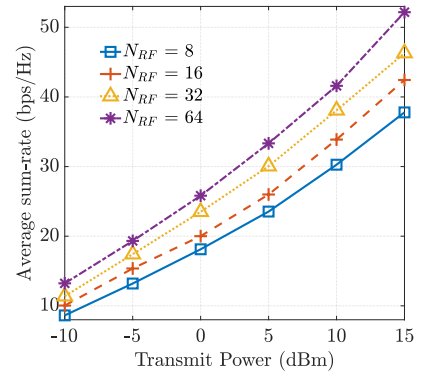


Fig. 3: Average per-subcarrier achievable sum-rate with different transmitter RF chain numbers and $S = 64$.

$$+ \mathbf{U}_{\text{RF},k}[a, m]\delta_{am}^{2*}. \quad (27)$$

To minimize the above expression subject to $|\mathbf{U}_{\text{RF},k}[a, m]| = 1$, we write $\mathbf{U}_{\text{RF},k}[a, m] = e^{\iota\nu}$ and substitute it in (27) as

$$\begin{aligned} & -e^{-\iota\nu}\delta_{am}^1 - e^{\iota\nu}\delta_{am}^{1*} + e^{-\iota\nu}\delta_{am}^2 + e^{\iota\nu}\delta_{am}^{2*} \\ &= e^{-\iota\nu}(\delta_{am}^2 - \delta_{am}^1) + e^{\iota\nu}(\delta_{am}^{2*} - \delta_{am}^{1*}) \\ &= e^{-\iota\nu}(\delta_{am}^2 - \delta_{am}^1) + e^{\iota\nu}(\delta_{am}^2 - \delta_{am}^1)^* = 2\Re[e^{-\iota\nu}(\delta_{am}^2 - \delta_{am}^1)] \end{aligned}$$

If we let $\Delta = \delta_{am}^2 - \delta_{am}^1 = |\Delta|e^{\iota\phi}$, then the objective function is $2\Re[e^{-\iota\nu}|\Delta|e^{\iota\phi}] = 2|\Delta|\Re[e^{\iota(\phi-\nu)}] = 2|\Delta|\cos(\phi-\nu)$. To minimize this expression, we need to minimize $\cos(\phi-\nu)$, which leads to $\phi-\nu = \pi$ and results in $\nu_{\text{opt}} = \phi - \pi = \arg(\delta_{am}^2 - \delta_{am}^1) - \pi$. Therefore, the optimal value is

$$\mathbf{U}_{\text{RF},k}[a, m] = e^{\iota[\arg(\delta_{am}^2 - \delta_{am}^1) - \pi]} = -\frac{\delta_{am}^2 - \delta_{am}^1}{|\delta_{am}^2 - \delta_{am}^1|}. \quad (28)$$

In the presence of the PS impairments at the user equipment that introduce random phase errors, one can use the robust optimization technique proposed for the RF precoder at the transmitter. We obtain the expectation with respect to the phase error from (27). Assuming $\mathbf{U}_{\text{RF},k} = \tilde{\mathbf{U}}_{\text{RF},k} \odot \mathbf{E}_{\text{error}}$. We note that $\mathbb{E}_{\mathbf{E}_{\text{error}}}[\mathbf{U}_{\text{RF},k}^*[a, m]\delta_{am}^1] = e^{-\sigma_e^2/2}\tilde{\mathbf{U}}_{\text{RF},k}^*[a, m]\delta_{am}^1$ and $\mathbb{E}_{\mathbf{E}_{\text{error}}}[\delta_{am}^2] = e^{-\sigma_e^2/2}\tilde{\delta}_{am}^2$ where

$$\tilde{\delta}_{am}^2 = \sum_{s \in \mathcal{S}} \sum_{\substack{i, j \\ (q, r) \neq (a, m)}} \mathbf{W}_k^s[i, j] \mathbf{U}_k^{s*}[m, j] \mathbf{O}_k^s[a, q] \tilde{\mathbf{U}}_{\text{RF},k}[q, r] \mathbf{U}_k^s[r, i].$$

Then, (27) is rewritten as $-e^{-\sigma_e^2/2}\tilde{\mathbf{U}}_{\text{RF},k}^*[a, m]\delta_{am}^1 - e^{-\sigma_e^2/2}\tilde{\mathbf{U}}_{\text{RF},k}[a, m]\delta_{am}^{1*} + e^{-\sigma_e^2}\tilde{\mathbf{U}}_{\text{RF},k}^*[a, m]\tilde{\delta}_{am}^2 + e^{-\sigma_e^2}\tilde{\mathbf{U}}_{\text{RF},k}[a, m]\tilde{\delta}_{am}^{2*}$. To minimize this expression, we deploy

$$\tilde{\mathbf{U}}_{\text{RF},k}[a, m] = -\frac{\tilde{\delta}_{am}^2 e^{-\sigma_e^2/2} - \delta_{am}^1}{|\tilde{\delta}_{am}^2 e^{-\sigma_e^2/2} - \delta_{am}^1|}.$$

F. The Proposed BCD-based Hybrid Precoding Approach

In the proposed hybrid precoding method, different blocks are updated in a cyclic order. When we update each block, we keep the rest of the blocks fixed. In the BCD method, \mathbf{U}_k^s

is updated using (10). \mathbf{W}_k^s is updated based on the equation given in Section IV-B. We update \mathbf{V}_k^s via the ADMM-based Algorithm 1. The PS matrix \mathbf{V}_{RF} is updated according to the method given in Section IV-D. Finally, the analog combiner is updated based on the mechanism given in Section IV-E. The proposed BCD approach converges to a stationary solution since each subproblem is solved to a stationary point [31]. The complexity analysis of the proposed methods is given in Appendix F.

V. SIMULATION RESULTS

In this section, we demonstrate the efficiency of the proposed methods via numerical simulations. We consider a downlink system with a transmitter having $N_t = 64$ antennas, and $K = 4$ users each equipped with $N_r = 4$ antennas and 2 RF chains. All four users share all subcarriers across a total bandwidth of 20 MHz, where the center frequency is 28 GHz. The users are randomly distributed in a circle of radius 4 meters, located 373 meters from the transmitter. The channel is modeled as a frequency-selective MIMO-OFDM channel with Rician fading, where each user k experiences a channel matrix $\mathbf{H}_k^s \in \mathbb{C}^{N_r \times N_t}$ on subcarrier s :

$$\begin{aligned} \mathbf{H}_k^s &= \sqrt{\frac{\kappa}{\kappa+1}} \sqrt{g_k} \mathbf{a}_r(\theta_k^{\text{AoA}}) \mathbf{a}_t^H(\theta_k^{\text{AoD}}) \\ &+ \sum_{\ell=1}^{T-1} \sqrt{\frac{1}{\kappa+1}} \sqrt{g_{k,\ell}} \mathbf{a}_r(\theta_{k,\ell}^{\text{AoA}}) \mathbf{a}_t^H(\theta_{k,\ell}^{\text{AoD}}) h_{k,\ell} e^{-j2\pi\ell s/S}, \end{aligned}$$

where the first term represents the dominant line-of-sight (LOS) component and the summation represents non-line-of-sight (NLOS) multipath components with $h_{k,\ell} \sim \mathcal{CN}(0, 1)$, and T is the number of channel taps. The Rician κ -factor is defined as the ratio of the power in the LOS component to the power in the scattered components as $\kappa = \frac{P_{\text{LOS}}}{P_{\text{NLOS}}} = 10^{\kappa_{\text{dB}}/10}$. Here, $\kappa_{\text{dB}} = 10$ dB. The path loss coefficients follow the 3GPP path loss model [32]. For the LOS component, we have $PL_{\text{dB}}^{\text{LOS}} = 22 \log_{10}(d_k) + 28 + 20 \log_{10}(f^c) + \xi_{\text{LOS}}$, where d_k is the distance in meters, f^c is the carrier frequency in GHz, $\xi_{\text{LOS}} \sim \mathcal{N}(0, \sigma_{\text{LOS}}^2)$ represents log-normal shadow fading with

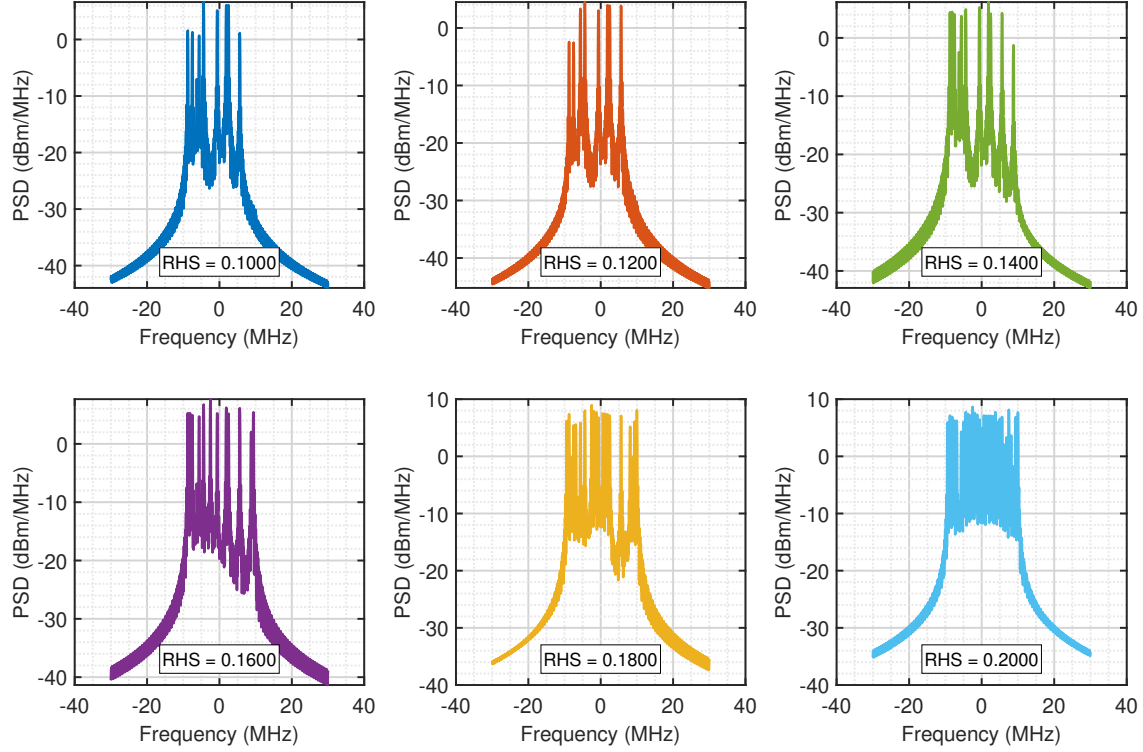


Fig. 4: The PSD of the transmitted 20-MHz-bandwidth OFDM symbol as the RHS of (7) changes.

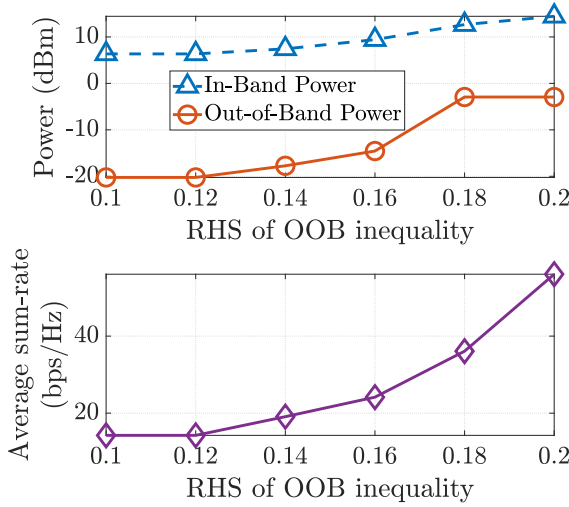


Fig. 5: The in-band/out-of-band emitted power and the achievable sum-rate versus the RHS of (7).

$\sigma_{\text{LOS}} = 5.8$ dB, and $g_k = 10^{-PL_{\text{dB}}^{\text{LOS}}/10}$. For the NLOS components $PL_{\text{dB}}^{\text{NLOS}} = 22 \log_{10}(d_k) + 28 + 20 \log_{10}(f^c) + \xi_{\text{NLOS}}$, where $\xi_{\text{NLOS}} \sim \mathcal{N}(0, \sigma_{\text{NLOS}}^2)$ with $\sigma_{\text{NLOS}} = 8.7$ dB, and $g_{k,\ell} = 10^{-PL_{\text{dB}}^{\text{NLOS}}/20}$ represents the channel gain amplitude.

The additive noise is modeled as spatially and temporally white complex Gaussian noise $\mathbf{n}_k^s \sim \mathcal{CN}(\mathbf{0}, \sigma_{\text{noise},k}^{s^2} \mathbf{I}_{N_r})$. The

noise power spectral density is -174 dBm/Hz. The noise figure of each user device is 8 dB.

The uniform linear array (ULA) response vectors are calculated as:

$$\begin{aligned} \mathbf{a}_t(\theta_k^{\text{AoD}}) &= [1, e^{j\psi}, e^{j2\psi}, \dots, e^{j(N_t-1)\psi}]^T, \\ \mathbf{a}_r(\theta_k^{\text{AoA}}) &= [1, e^{j\psi'}, e^{j2\psi'}, \dots, e^{j(N_r-1)\psi'}]^T, \end{aligned}$$

where the phase progressions are $\psi = \frac{2\pi d_t \sin(\theta_k^{\text{AoD}})}{\lambda}$ and $\psi' = \frac{2\pi d_r \sin(\theta_k^{\text{AoA}})}{\lambda}$, with d_t and d_r being the inter-element spacing (typically $\lambda/2 = 5.35$ mm), θ_k^{AoD} and θ_k^{AoA} the angles of departure and arrival respectively, and λ the wavelength.

For NLOS components, the angles are randomly distributed around the main LOS angles with angular spread σ_θ as $\theta_{k,\ell}^{\text{AoD}} = \theta_k^{\text{AoD}} + \Delta\theta_{k,\ell}$, $\theta_{k,\ell}^{\text{AoA}} = \theta_k^{\text{AoA}} + \Delta\phi_{k,\ell}$, where $\Delta\theta_{k,\ell}, \Delta\phi_{k,\ell} \sim \mathcal{N}(0, \sigma_\theta^2)$.

The maximum allowed amplitude of the unclipped signal is $\chi = 8.2$, and the clipping constraint (6) is satisfied with a probability of at least 70%. To avoid OOB emissions, we set the notched frequencies from -29 MHz to -10.1 MHz and 10.1 MHz to 29 MHz in increments of 50 Hz. The right-hand side (RHS) of (7) is set to 1. With 32 subcarriers, we plot the per-subcarrier convergence of the proposed BCD algorithm for different numbers of RF chains in Fig. 1, where the per-subcarrier power budget is 5 dBm. We observe that the algorithm's achievable rate increases monotonically with each iteration. Even though five subproblems $(\mathbf{U}_{\text{RF},k}, \mathbf{V}_{\text{RF}}, \mathbf{U}_k, \mathbf{V}_k, \mathbf{W}_k)$ are solved at each iteration, the

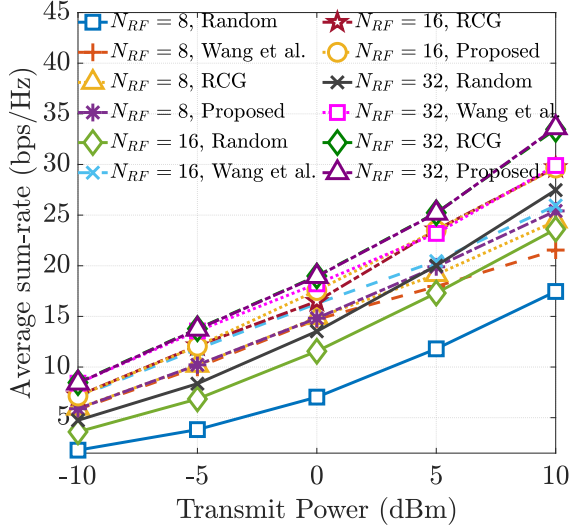


Fig. 6: The average per-subcarrier sum-rate of different hybrid precoding methods.

BCD method converges after only a few iterations. Moreover, the average per-subcarrier achievable sum-rate increases as the number of RF chains grows.

The average per-subcarrier achievable sum-rate across the users is shown for 32 and 64 subcarriers in Figs. 2 and 3, respectively. The per-subcarrier transmit power budget is varied from -10 dBm to 15 dBm in increments of 5 dB. The average per-subcarrier achievable sum-rate increases with higher transmit power budgets and a greater number of RF chains. The average per-subcarrier achievable sum-rate is higher for 64 subcarriers than for 32 subcarriers. This is due to the fact that with 64 subcarriers, the subcarrier bandwidth is halved (312.5 kHz compared to 625 kHz), which in turn reduces the noise power per subcarrier at each receive antenna by half.

Next, we demonstrate how OOB emissions vary with notching frequencies. The probability of maintaining the clipping constraint is 70% , and $\chi = 10$. The number of subcarriers is 32. We show the PSD of the transmitted 20 MHz OFDM symbol in Fig. 4, while varying the RHS of (7). It is observed that as the RHS of (7) increases, both the allowable transmit power and the width of the OFDM symbol's PSD increase.

The in-band emissions, OOB emissions, and the average per-subcarrier achievable sum-rate are depicted in Fig. 5, where $P^s = 24$ dBm and $N_{RF} = 32$. The optimized hybrid precoding results in 6.3 dBm of in-band emissions and -20.2 dBm of OOB emissions when the RHS of (7) is 0.1 . The average per-subcarrier sum-rate is 14.2 bps/Hz. When the RHS of (7) is increased to 0.14 , the in-band emissions rise to 7.4 dBm, and the OOB emissions increase to -17.7 dBm. Consequently, the average per-subcarrier sum-rate increases to 19 bps/Hz. Therefore, increasing the RHS of (7) results in higher OOB emissions and an improved average per-subcarrier sum-rate. Additional data points are shown in Fig. 5 as the RHS of (7) is incrementally increased.

We compare our proposed RF precoding-combination

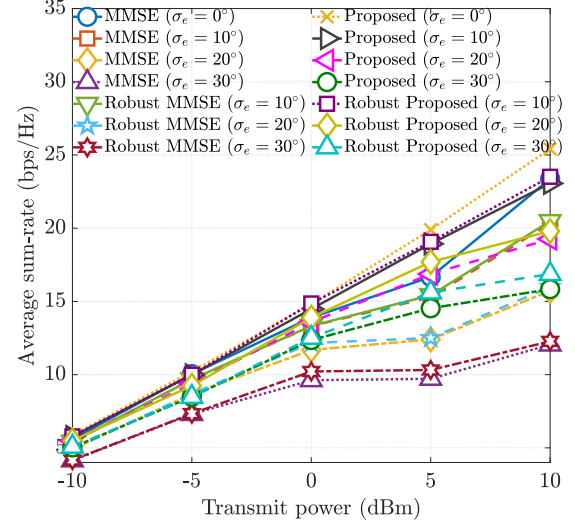


Fig. 7: The achievable per-subcarrier sum-rate of the classical hybrid MMSE and the proposed BCD methods in the presence of different PS noise levels when $N_{RF} = 8$.

scheme with the method presented in Wang *et al.* [33]. This reference employs a coordinate descent algorithm that iteratively minimizes the objective function. In this algorithm, individual PSs at the transmitter or for a specific user are alternately optimized via a numerical search method, while all other PS values are held constant. We also demonstrate the performance of the RCG method given in the appendix and also studied in [2], [4] in Fig. 6. The random assignment of PS values for the precoder and combiners is additionally considered. As illustrated in Fig. 6, which depicts the performance across varying numbers of RF chains, the proposed method outperforms these benchmark approaches in terms of average sum-rate, with RCG demonstrating comparable performance.

When $\mathbf{W}_k^s = \mathbf{I}_{n_k}$, the proposed method simplifies to the hybrid MMSE precoding/combing method. With ideal noise-free PSs ($\sigma_e = 0^\circ$), we compare the performance of the proposed and MMSE methods in Figs. 7 and 8 for $N_{RF} = 8$ and $N_{RF} = 16$, respectively. It is observed that the proposed algorithm achieves higher average sum-rates compared to the hybrid MMSE method. Different levels of noise strength is considered $\sigma_e = [10^\circ, 20^\circ, 30^\circ]$. From Figs. 7 and 8, it is observed that phase noise of PSs degrade the average sum-rate of the system. When the proposed robust PS update rules are deployed, given algorithms outperform non-robust versions (either proposed or MMSE) in the presence of PS impairments.

VI. CONCLUDING REMARKS

In this paper, we studied the hybrid digital-RF precoding design for MU-MIMO-OFDM systems with possibly impaired PSs subject to constraints on PAPR, OOB emissions and clipping. We proposed a WMMSE-based BCD method to maximize the sum-rate of users. A problem decomposition and an ADMM approach were proposed to optimize the digital precoder of the transmitter, where the solutions for the ADMM subproblems were obtained through closed-forms and

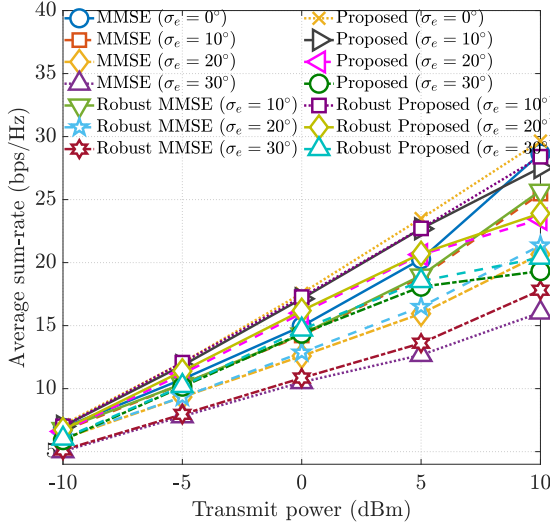


Fig. 8: The achievable per-subcarrier sum-rate of the classical hybrid MMSE and the proposed BCD methods in the presence of different PS noise levels when $N_{RF} = 16$.

bisection searches. Coordinate descent methods with closed-form updates were proposed to optimize the phase shifts at the transmitter and users, where the unit modulus constraints are considered for PSs. Optimizing with respect to different blocks with the Gauss-Seidel rule is continued until all blocks converge. We demonstrated the efficiency and efficacy of the proposed approaches against classical methods via extensive simulations.

REFERENCES

- [1] F. Sohrabi and W. Yu, "Hybrid analog and digital beamforming for mmWave OFDM large-scale antenna arrays," *IEEE J. Sel. Areas in Commun.*, vol. 35, no. 7, pp. 1432–1443, Apr. 2017.
- [2] X. Yu, J.C. Shen, J. Zhang, and K.B. Letaief, "Alternating minimization algorithms for hybrid precoding in millimeter wave MIMO systems," *IEEE J. Sel. Topics Signal Proces.*, vol. 10, no. 3, pp. 485–500, fEB. 2016.
- [3] L. Liang, W. Xu, and X. Dong, "Low-complexity hybrid precoding in massive multiuser MIMO systems," *IEEE Wireless Commun. Lett.*, vol. 3, no. 6, pp. 653–656, Oct. 2014.
- [4] X. Zhao, T. Lin, Y. Zhu, and J. Zhang, "Partially-connected hybrid beamforming for spectral efficiency maximization via a weighted MMSE equivalence," *IEEE Trans. Wireless Commun.*, vol. 20, no. 12, pp. 8218–8232, Jul. 2021.
- [5] A. Tom, A. Şahin, and H. Arslan, "Suppressing alignment: Joint PAPR and out-of-band power leakage reduction for OFDM-based systems," *IEEE Trans. Commun.*, vol. 64, no. 3, pp. 1100–1109, Dec. 2016.
- [6] J. Galaviz-Aguilar V. Alejandro, T. Cesar, and E. Tlelo-Cuaute, "RF-PA modeling of PAPR: A precomputed approach to reinforce spectral efficiency," *IEEE Access*, vol. 8, pp. 138217–138235, Jul. 2020.
- [7] S. Liu, Y. Wang, Z. Lian, Y. Su, and Z. Xie, "Joint suppression of PAPR and OOB radiation for OFDM systems," *IEEE Trans. Broadcasting*, vol. 69, no. 2, pp. 528–537, Feb. 2023.
- [8] S. Kant, M. Bengtsson, B. Göransson, G. Fodor, and C. Fischione, "Efficient optimization for large-scale MIMO-OFDM spectral precoding," *IEEE Trans. Wireless Commun.*, vol. 20, no. 9, pp. 5496–5513, Sep. 2021.
- [9] Y.-C. Wang and Z.-Q. Luo, "Optimized iterative clipping and filtering for PAPR reduction of OFDM signals," *IEEE Trans. Commun.*, vol. 59, no. 1, pp. 33–37, Jan. 2011.
- [10] S. Wan, S. Hu, K. Kang, X. Luo, and H. Qian, "A novel PAPR reduction method for hybrid beamforming transmitter," *Digital Signal Process.*, vol. 136, pp. 103974, 2023.
- [11] R. Zayani, J.-B. Doré, B. Misopein, and D. Demmer, "Local PAPR-aware precoding for energy-efficient cell-free massive MIMO-OFDM systems," *IEEE Trans. Green Commun. Netw.*, vol. 7, no. 3, pp. 1267–1284, Mar. 2023.
- [12] S. Kant, M. Bengtsson, G. Fodor, B. Göransson, and C. Fischione, "EVM mitigation with PAPR and ACLR constraints in large-scale MIMO-OFDM using TOP-ADMM," *IEEE Trans. Wireless Commun.*, vol. 21, no. 11, pp. 9460–9481, Nov. 2022.
- [13] X. Zhu, W. Pan, H. Li, and Y. Tang, "Simplified approach to optimized iterative clipping and filtering for PAPR reduction of ofdm signals," *IEEE Trans. Commun.*, vol. 61, no. 5, pp. 1891–1901, Feb. 2013.
- [14] R. Zayani, H. Shaék, and D. Roviras, "Ping-pong joint optimization of PAPR reduction and HPA linearization in OFDM systems," *IEEE Trans. Broadcast.*, vol. 65, no. 2, pp. 308–315, Jul. 2019.
- [15] J. Van De Beek, "Sculpting the multicarrier spectrum: a novel projection precoder," *IEEE Commun. Lett.*, vol. 13, no. 12, pp. 881–883, Dec. 2009.
- [16] A. Tom, A. Sahin, and H. Arslan, "Mask compliant precoder for OFDM spectrum shaping," *IEEE Commun. Lett.*, vol. 17, no. 3, pp. 447–450, Mar. 2013.
- [17] R. Kumar and A. Tyagi, "Computationally efficient mask-compliant spectral precoder for OFDM cognitive radio," *IEEE Trans. Cognit. Commun. Netw.*, vol. 2, no. 1, pp. 15–23, Mar. 2016.
- [18] S. Kant, M. Bengtsson, G. Fodor, B. Göransson, and C. Fischione, "EVM-constrained and mask-compliant MIMO-OFDM spectral precoding," *IEEE Trans. Wireless Commun.*, vol. 20, no. 1, pp. 590–606, Jan. 2021.
- [19] T. Taheri, M. Mohamad, R. Nilsson, and J. van de Beek, "Joint spectral-spatial precoders in MIMO-OFDM transmitters," *Signal Process.*, vol. 172, pp. 107538, Jul. 2020.
- [20] M. Joham, W. Utschick, and J.A. Nossek, "Linear transmit processing in MIMO communications systems," *IEEE Trans. Signal Process.*, vol. 53, no. 8, pp. 2700–2712, Aug. 2005.
- [21] Q. Shi, M. Razaviyayn, Z.-Q. Luo, and C. He, "An iteratively weighted MMSE approach to distributed sum-utility maximization for a MIMO interfering broadcast channel," *IEEE Trans. Signal Process.*, vol. 59, no. 9, pp. 4331–4340, Sep. 2011.
- [22] D. Nguyen, L. Le Bao, T. Le-Ngoc, and R.W. Heath, "Hybrid MMSE precoding and combining designs for mmWave multiuser systems," *IEEE Access*, vol. 5, pp. 19167–19181, 2017.
- [23] R. Garg and A. S. Natarajan, "A 28-GHz low-power phased-array receiver front-end with 360° RTPS phase shift range," *IEEE Trans. Microw. Theory Tech.*, vol. 65, no. 11, pp. 4703–4714, Jun. 2017.
- [24] C.W. Byeon and C.S. Park, "A low-loss compact 60-GHz phase shifter in 65-nm CMOS," *IEEE Microw. Wireless Compon. Lett.*, vol. 27, no. 7, pp. 663–665, Jun. 2017.
- [25] W. Wang, H. Yin, X. Chen, and W. Wang, "Robust and low-overhead hybrid beamforming design with imperfect phase shifters in multi-user millimeter wave systems," *IEEE Access*, vol. 8, pp. 74002–74014, May 2020.
- [26] J. Li, Z. Wang, Y. Zhang, P. Zhu, D. Wang, and X. You, "Robust hybrid beamforming for outage-constrained multigroup multicast mmWave transmission with phase shifter impairments," *IEEE Syst. J.*, vol. 17, no. 1, pp. 869–880, Mar. 2023.
- [27] D. Mishra and H. Johansson, "Optimal channel estimation for hybrid energy beamforming under phase shifter impairments," *IEEE Trans. Commun.*, vol. 67, no. 6, pp. 4309–4325, Jun. 2019.
- [28] S. Gong, C. Xing, V. Lau, S. Chen, and L. Hanzo, "Majorization-minimization aided hybrid transceivers for MIMO interference channels," *IEEE Trans. Signal Proces.*, vol. 68, pp. 4903–4918, Aug. 2020.
- [29] S. Boyd, "Convex optimization," *Cambridge UP*, 2004.
- [30] S. Boyd, N. Parikh, E. Chu, B. Peleato, and J. Eckstein, "Distributed optimization and statistical learning via the alternating direction method of multipliers," *Foundations and Trends® in Machine learning*, vol. 3, no. 1, pp. 1–122, 2011.
- [31] D. P. Bertsekas, *Nonlinear Programming*, Athena Scientific, 3rd ed., 2016.
- [32] 3GPP TR 36.814, "Further advancements for E-UTRA physical layer aspects," Tech. Rep., 3rd Generation Partnership Project (3GPP), Mar. 2017, Release 9, V9.2.0.
- [33] Z. Wang, M. Li, Q. Liu, and A. L. Swindlehurst, "Hybrid precoder and combiner design with low-resolution phase shifters in mmWave MIMO systems," *IEEE J. Sel. Topics Signal Proces.*, vol. 12, pp. 256–269, 2018.
- [34] J.M. Lee, *Smooth manifolds*, Springer, 2012.
- [35] P.-A Absil, R. Mahony, and R. Sepulchre, *Optimization algorithms on matrix manifolds*, Princeton University Press, 2008.

APPENDIX A PROOF OF PROPOSITION 1

Let us start with fully-digital systems. We reformulate the PAPR constraint into ℓS individual constraints:

$$\frac{|\mathbf{x}^a[n]|^2}{\mathbb{E}[\|\mathbf{x}^a\|_2^2]} \leq \text{PAPR}_{\max}, \quad n \in \{1, \dots, \ell S\}.$$

To calculate the expectation of $|\mathbf{x}^a[n]|^2$, one can use the diagonal elements of the following matrix:

$$\begin{aligned} \mathbb{E}[\mathbf{x}^a \mathbf{x}^{a^H}] &= \mathbb{E}[\mathbf{F}^{-1} \mathbf{g}^a \mathbf{g}^{a^H} \mathbf{F}^{-1^H}] = \mathbf{F}^{-1} \mathbb{E}[\mathbf{g}^a \mathbf{g}^{a^H}] \mathbf{F}^{-1^H} \\ &\stackrel{(a)}{=} \mathbf{F}^{-1} \\ &\text{diag} \left(\sum_{k=1}^K \|\mathbf{V}_k^{-S/2}[a, :] \|_2^2, \dots, \sum_{k=1}^K \|\mathbf{V}_k^{S/2}[a, :] \|_2^2 \right) \mathbf{F}^{-1^H}, \end{aligned}$$

where (a) follows from the fact that $\mathbb{E}[\boldsymbol{\omega}_k^s \boldsymbol{\omega}_k^{s^H}] = \mathbf{I}_{n_k}$ and $\mathbb{E}[\boldsymbol{\omega}_k^s \boldsymbol{\omega}_{k^H}^{s^H}] = \mathbf{0}_{n_k}$ if $s' \neq s$. The $(n, n)^{\text{th}}$ element of $\mathbb{E}[\mathbf{x}^a \mathbf{x}^{a^H}]$ can be written as $\sigma_x^2 = \sum_{s \in \mathcal{S}} \sum_{k=1}^K \|\mathbf{V}_k^s[a, :] \|_2^2$. Given that $\mathbf{F}^{-1^H} \mathbf{F}^{-1} / \ell S = \mathbf{I}_S$, we substitute $\mathbb{E}[\|\mathbf{x}^a\|_2^2]$ by its expansion $\sum_{j=1}^{\ell S} \mathbb{E}[|\mathbf{x}^a[j]|^2] = \text{tr}(\mathbb{E}[\mathbf{x}^a \mathbf{x}^{a^H}]) = \ell S \sum_{s \in \mathcal{S}} \sum_{k=1}^K \|\mathbf{V}_k^s[a, :] \|_2^2$, yielding

$$|\mathbf{x}^a[n]| \leq \sqrt{\text{PAPR}_{\max} \ell S \sum_{s \in \mathcal{S}} \sum_{k=1}^K \|\mathbf{V}_k^s[a, :] \|_2^2}.$$

We note that $\mathbf{x}^a[n]$ is a zero-mean complex Gaussian random variable. Therefore, $|\mathbf{x}^a[n]|$ is a Rayleigh random variable. The cumulative distribution function (CDF) of the Rayleigh distribution can be used to calculate the probability that the inequality holds with at least $1 - \epsilon$ probability, as follows:

$$1 - \epsilon \leq 1 - e^{-\ell S \text{PAPR}_{\max} \sum_{s \in \mathcal{S}} \sum_{k=1}^K \|\mathbf{V}_k^s[a, :] \|_2^2 / 2 \sum_{s \in \mathcal{S}} \sum_{k=1}^K \|\mathbf{V}_k^s[a, :] \|_2^2},$$

where the CDF of a Rayleigh distribution is $F(x) = 1 - e^{-x^2/(2\sigma^2)}$. The above inequality can be simplified as follows:

$$e^{-\ell S \text{PAPR}_{\max} / 2} \leq \epsilon$$

Therefore, by increasing the oversampling factor, one can satisfy the PAPR constraint.

Here, we consider the partially-connected hybrid system. We note that \mathbf{w}^a is the vector of signals in different subcarriers at the m^{th} RF chain before the iFFT. Moreover, \mathbf{V}_{RF} does not affect the magnitudes of the entries of \mathbf{w}^a and just applies phase rotations. The matrix $\mathbf{F}^{-1} / \sqrt{\ell S}$ is a left unitary, i.e., $\mathbf{F}^{-1^H} \mathbf{F}^{-1} / \ell S = \mathbf{I}_S$. The expectation of $|\mathbf{x}^a[n]|^2$ can be calculated using the diagonal terms of $\mathbb{E}[\mathbf{x}^a \mathbf{x}^{a^H}]$, which is similar to that of fully-digital systems since $|\mathbf{V}_{\text{RF}}[a, m]| = 1$. Due to the same reason, we have $\mathbb{E}[|\mathbf{x}^a[n]|^2] = \sum_{k=1}^K \sum_{s \in \mathcal{S}} \|\mathbf{V}_{\text{RF}}[a, :] \mathbf{V}_k^s\|_2^2 = \sum_{k=1}^K \sum_{s \in \mathcal{S}} \|\mathbf{V}_k^s[m, :] \|_2^2$. Therefore, one can use the same constraint for the fully-digital systems for the partially-connected hybrid systems as well.

APPENDIX B PROOF OF PROPOSITION 2

We start with fully-digital systems. To address the clipping constraint, we reformulate it as ℓS individual constraints:

$$|\mathbf{x}^a[n]| \leq \chi, \quad n \in \{1, \dots, \ell S\}, \quad \forall a.$$

Since the intended symbols to users are zero-mean complex Gaussian variables, we have $\mathbb{E}[\mathbf{F}^{-1} \mathbf{g}^a] = \mathbf{0}$. We note that $|\mathbf{x}^a[n]|$ follows a Rayleigh distribution. We aim to satisfy $\mathbb{P}(|\mathbf{x}^a[n]| \geq \chi) \leq \epsilon$. The $(n, n)^{\text{th}}$ element of $\mathbb{E}[\mathbf{x}^a \mathbf{x}^{a^H}]$ can be written as $\sigma_x^2 = \sum_{s \in \mathcal{S}} \sum_{k=1}^K \|\mathbf{V}_k^s[a, :] \|_2^2$. Therefore, to ensure $|\mathbf{x}^a[n]| \leq \chi$ with probability at least $1 - \epsilon$, we should have

$$\mathbb{P}(|\mathbf{x}^a[n]| > \chi) \leq \epsilon.$$

Using the Rayleigh distribution CDF, we obtain

$$\exp \left(-\frac{\chi^2}{2\sigma_x^2} \right) \leq \epsilon.$$

After one simplifies the above expression and substitutes the expansion for σ_x^2 , we obtain

$$\sqrt{-2 \ln(\epsilon) \left(\sum_{k=1}^K \sum_{s \in \mathcal{S}} \|\mathbf{V}_k^s[a, :] \|_2^2 \right)} \leq \chi.$$

To revise the above inequality for the fully-digital precoding and obtain an inequality for the hybrid precoding, we utilize the fact that each non-zero element of \mathbf{V}_{RF} has an absolute value of one. Suppose that the a^{th} antenna is connected to the m^{th} RF chain. Similar to the previous case, $\mathbb{E}[\mathbf{F}^{-1} \mathbf{w}^a] = \mathbf{0}$. Moreover, we have $\mathbf{x}^a = \mathbf{F}^{-1} \mathbf{w}^a$. To calculate $\mathbb{E}[|\mathbf{x}^a[n]|^2]$, one can use the $(n, n)^{\text{th}}$ element of $\mathbb{E}[\mathbf{x}^a \mathbf{x}^{a^H}] = \mathbf{F}^{-1} \mathbb{E}[\mathbf{w}^a \mathbf{w}^{a^H}] \mathbf{F}^{-1^H}$. Since $\mathbb{E}[\mathbf{w}^a \mathbf{w}^{a^H}]$ is diagonal, $\mathbb{E}[|\mathbf{x}^a[n]|^2] = \sum_{k=1}^K \sum_{s \in \mathcal{S}} \|\mathbf{V}_{\text{RF}}[a, :] \mathbf{V}_k^s\|_2^2 = \sum_{k=1}^K \sum_{s \in \mathcal{S}} \|\mathbf{V}_k^s[m, :] \|_2^2$. Then, the equivalent bound to calculate the probability of clipping is as given in (6).

APPENDIX C PROOF OF PROPOSITION 3

We start with fully-digital systems. Assuming that the variables $\boldsymbol{\omega}_k^s$ are complex Gaussian distributed and independent across different values of k , the expectation of $\mathbf{z}^a \triangleq \mathbf{A} \mathbf{g}^a$ is zero because it is a linear combination of $\boldsymbol{\omega}_k^s$. The covariance matrix of \mathbf{z}^a can be expressed as

$$\Sigma_{\mathbf{z}^a} = \mathbb{E}(\mathbf{z}^a \mathbf{z}^{a^H}) = \mathbf{A} \Sigma_{\mathbf{g}^a} \mathbf{A}^H,$$

where

$$\Sigma_{\mathbf{g}^a} = \text{diag}((\zeta^{-S/2})^2, \dots, (\zeta^{S/2})^2)$$

and ζ^{s^2} for $s \in \{-S/2, \dots, S/2\}$ is defined as

$$\zeta^{s^2} = \sum_{k=1}^K \mathbf{V}_k^s[a, :] \mathbb{E}[\boldsymbol{\omega}_k^s (\boldsymbol{\omega}_k^s)^H] (\mathbf{V}_k^s[a, :])^H = \sum_{k=1}^K \|\mathbf{V}_k^s[a, :] \|_2^2.$$

To ensure that the complex random vector \mathbf{z}^a remains close to its expected value with high probability, we apply Chebyshev's inequality. Specifically, the probability that the

Algorithm 2: The Proposed Riemannian Conjugate Gradient (RCG) Algorithm for RF Precoding

Input: $\mathbf{v}_{\text{PS}}^0 \in \mathcal{M}$;
 Initialize $\tau \leftarrow 0$;
 Set the initial search direction $\boldsymbol{\eta}^0 \leftarrow -\zeta(\mathbf{v}_{\text{PS}}^0)$;
while $\mathbf{v}_{\text{PS}}^\tau$ not converged **do**
 Perform Armijo backtracking line search to find α_1 ;
 Update $\mathbf{v}_{\text{PS}}^{\tau+1} \leftarrow \text{Retr}_{\mathbf{v}_{\text{PS}}^\tau}(\alpha_1 \boldsymbol{\eta}^\tau)$;
 Compute new Riemannian gradient $\zeta(\mathbf{v}_{\text{PS}}^{\tau+1})$;
 Compute Polak-Ribiere parameter α_2 ;
 Perform vector transport $T_{\mathbf{v}_{\text{PS}}^\tau \rightarrow \mathbf{v}_{\text{PS}}^{\tau+1}}(\boldsymbol{\eta}^\tau)$;
 Update the search direction $\boldsymbol{\eta}^{\tau+1}$ with (30) ;
 $\tau \leftarrow \tau + 1$;
Output: $\mathbf{v}_{\text{PS}}^{\text{opt}} = \mathbf{v}_{\text{PS}}^\tau$;

squared norm of the deviation of \mathbf{z}^a from its mean exceeds ϵ_1 is bounded by

$$\mathbb{P}(\|\mathbf{z}^a - \mathbb{E}[\mathbf{z}^a]\|_2^2 \geq \epsilon_1) \leq \frac{\varsigma^2}{\epsilon_1^2},$$

where $\varsigma^2 = \text{tr}(\mathbb{E}[\mathbf{z}^a \mathbf{z}^{a^H}])$. Substituting the mean $\mathbb{E}[\mathbf{z}^a]$ and the variance ς^2 we have

$$\begin{aligned} \mathbb{P}(\|\mathbf{z}^a\|_2^2 \geq \epsilon_1) &\leq \frac{\text{tr}(\mathbf{A} \text{diag}((\varsigma^{-S/2})^2, \dots, (\varsigma^{S/2})^2) \mathbf{A}^H)}{\epsilon_1^2} \\ &= \frac{\text{tr}(\text{diag}((\varsigma^{-S/2})^2, \dots, (\varsigma^{S/2})^2) \mathbf{L})}{\epsilon_1^2} \\ &= \frac{\sum_{s \in \mathcal{S}} \varsigma^s \mathbf{L}[s, s]}{\epsilon_1^2} \leq \epsilon_2, \end{aligned}$$

where $\mathbf{L}[s, s]$ represents the (s, s) th elements of the matrix $\mathbf{L} = \mathbf{A}^H \mathbf{A}$. The following constraint ensures that the probability of the squared norm of the residual of $\mathbf{A}\mathbf{g}^a = \mathbf{0}$ being less than ϵ_1 is at least $1 - \epsilon_2$:

$$\sqrt{\sum_{s \in \mathcal{S}} \mathbf{L}[s, s] \left(\sum_{k=1}^K (\|\mathbf{V}_k^a[a, :] \|_2^2) \right)} \leq \epsilon_1 \sqrt{\epsilon_2}, \quad \forall a.$$

We consider partially connected systems. When antenna a is connected to the m th RF chain, we have

$$\mathbf{w}^a = \begin{bmatrix} \sum_{k=1}^K \mathbf{V}_{\text{RF}}[a, m] \mathbf{V}_k^{-S/2} [m, :] \boldsymbol{\omega}_k^{-S/2} \\ \vdots \\ \sum_{k=1}^K \mathbf{V}_{\text{RF}}[a, m] \mathbf{V}_k^{S/2} [m, :] \boldsymbol{\omega}_k^{S/2} \end{bmatrix}$$

and $\mathbf{V}_{\text{RF}}[a, m]$ is canceled in $\mathbf{w}^a \mathbf{w}^{a^H}$. Therefore, (7) is obtained.

APPENDIX D
RIEMANNIAN CONJUGATE GRADIENT FOR PRECODING

Fixing other blocks, the subproblem with respect to \mathbf{v}_{PS} is convex. The main challenge arises from the unit-modulus constraints on \mathbf{v}_{PS} , which form a complex sphere manifold $\mathcal{M} = \{\mathbf{v}_{\text{PS}} \in \mathbb{C}^{N_t \times 1} : |\mathbf{v}_{\text{PS}}[i]| = 1, 1 \leq i \leq N_t\}$. We

utilize the RCG algorithm, a method frequently employed in the development of hybrid beamforming systems. The RCG algorithm involves several key steps as follows: calculating the Riemannian gradient, retraction, performing vector transport, and determining the search direction. Here is a list of required steps in the proposed RCG algorithm:

1) *Compute the Riemannian Gradient:* For a given τ^{th} iterate $\mathbf{v}_{\text{PS}}^\tau$, the Riemannian gradient is the orthogonal projection of the Euclidean gradient of $\sum_{s \in \mathcal{S}} \sum_{k=1}^K \text{tr}(\mathbf{W}_k^s \mathbf{E}_k^s)$ onto the tangent space $T_{\mathbf{v}_{\text{PS}}^\tau} \mathcal{M}$ of the manifold \mathcal{M} at $\mathbf{v}_{\text{PS}}^\tau$. The tangent space is defined as

$$T_{\mathbf{v}_{\text{PS}}^\tau} \mathcal{M} = \{\mathbf{v}_{\text{PS}} \in \mathbb{C}^{N_t \times 1} : \Re(\mathbf{v}_{\text{PS}} \odot \mathbf{v}_{\text{PS}}^*) = \mathbf{0}\},$$

where $(\cdot)^*$ denotes the conjugation. The tangent space is defined locally at each point on the manifold. Since the neighborhood around each point on a manifold is similar to the Euclidean space, optimization algorithms designed for Euclidean spaces can be locally applied to Riemannian manifolds as well. The tangent space offers a convenient vector space for solving optimization problems, allowing for the use of certain line search methods. Building on this idea, we propose a conjugate gradient algorithm based on Riemannian manifold optimization. This allows us to employ manifold optimization techniques, specifically an RCG algorithm to solve the problem to a critical point [2], [34], [35]. The Euclidean gradient at $\mathbf{v}_{\text{PS}}^\tau$ is

$$\nabla f(\mathbf{v}_{\text{PS}}^\tau) = \mathbf{Q}_{\text{PS}} \mathbf{v}_{\text{PS}}^\tau - \mathbf{u}_{\text{PS}}. \quad (29)$$

The Riemannian gradient is then

$$\zeta(\mathbf{v}_{\text{PS}}^\tau) = \nabla f(\mathbf{v}_{\text{PS}}^\tau) - \Re\{\nabla f(\mathbf{v}_{\text{PS}}^\tau) \odot \mathbf{v}_{\text{PS}}^*\} \odot \mathbf{v}_{\text{PS}}^\tau.$$

2) *Retraction:* Retraction is one crucial component in manifold optimization that transports a vector from the tangent space back onto the manifold. It determines the point on the manifold reached when moving along a tangent vector. Let us denote the search direction at the τ^{th} iteration by $\boldsymbol{\eta}^\tau$, which can be initialized as $\boldsymbol{\eta}^0 = -\zeta(\mathbf{v}_{\text{PS}}^0)$. The retraction of a tangent vector $\alpha_1 \boldsymbol{\eta}^\tau$, α_1 being the momentum parameter, at a point $\mathbf{v}_{\text{PS}}^\tau \in \mathcal{M}$ can be expressed as follows:

$$\text{Retr}_{\mathbf{v}_{\text{PS}}^\tau} : T_{\mathbf{v}_{\text{PS}}^\tau} \mathcal{M} \mapsto \mathcal{M} :$$

$$\alpha_1 \boldsymbol{\eta}^\tau \mapsto \mathbf{v}_{\text{PS}}^{\tau+1} = \text{Retr}_{\mathbf{v}_{\text{PS}}^\tau}(\alpha_1 \boldsymbol{\eta}^\tau) = \text{vec} \left(\left\{ \frac{\mathbf{v}_{\text{PS}}^\tau[i] + \alpha_1 \boldsymbol{\eta}^\tau[i]}{|\mathbf{v}_{\text{PS}}^\tau[i] + \alpha_1 \boldsymbol{\eta}^\tau[i]|} \right\}_i \right).$$

Each momentum parameter calculation α_1 is determined by the Armijo backtracking line search, which finds the maximum $\alpha_1 = \beta^i, i \in \{0, 1, \dots\}$, such that the below inequality is satisfied:

$$f(\mathbf{v}_{\text{PS}}^\tau) - f(\text{Retr}_{\mathbf{v}_{\text{PS}}^\tau}(\alpha_1 \boldsymbol{\eta}^\tau)) \geq -c\alpha_1 \zeta(\mathbf{v}_{\text{PS}}^\tau)^H \boldsymbol{\eta}^\tau,$$

where $c \in (0, 0.5)$ and $\beta \in (0, 1)$.

3) *Update the Search direction:* We employ the conjugate gradient method, where the search direction is updated as follows:

$$\boldsymbol{\eta}^{\tau+1} = -\zeta(\mathbf{v}_{\text{PS}}^{\tau+1}) + \alpha_2 T_{\mathbf{v}_{\text{PS}}^\tau \rightarrow \mathbf{v}_{\text{PS}}^{\tau+1}}(\boldsymbol{\eta}^\tau). \quad (30)$$

When moving to a new point via retraction, we move to a new location on the manifold with a different tangent space.

Thus, η^τ and $\eta^{\tau+1}$ exist in distinct tangent spaces, meaning they cannot be directly combined. As a result, the transport operation $T_{\mathbf{v}_{\text{PS}}^\tau \rightarrow \mathbf{v}_{\text{PS}}^{\tau+1}}(\eta^\tau)$ is needed to transfer the previous search direction from its tangent space to the one at the new point $\eta^{\tau+1}$. This transport operation is defined as follows:

$$T_{\mathbf{v}_{\text{PS}}^\tau \rightarrow \mathbf{v}_{\text{PS}}^{\tau+1}}(\eta^\tau) : T_{\mathbf{v}_{\text{PS}}^\tau} \mathcal{M} \mapsto T_{\mathbf{v}_{\text{PS}}^{\tau+1}} \mathcal{M} : \\ \eta^\tau \mapsto \eta^\tau - \Re\{\eta^\tau \odot \mathbf{v}_{\text{PS}}^{\tau+1}\} \odot \mathbf{v}_{\text{PS}}^{\tau+1}.$$

Using the above definition, (30) can be rewritten as

$$\eta^{\tau+1} = -\zeta(\mathbf{v}_{\text{PS}}^{\tau+1}) + \alpha_2(\eta^\tau - \Re\{\eta^\tau \odot \mathbf{v}_{\text{PS}}^{\tau+1}\} \odot \mathbf{v}_{\text{PS}}^{\tau+1}),$$

where α_2 is the Polak-Ribiere parameter, calculated as

$$\alpha_2 = \frac{\zeta(\mathbf{v}_{\text{PS}}^{\tau+1})^H(\zeta(\mathbf{v}_{\text{PS}}^{\tau+1}) - \zeta(\mathbf{v}_{\text{PS}}^\tau))}{\zeta(\mathbf{v}_{\text{PS}}^\tau)^H \zeta(\mathbf{v}_{\text{PS}}^\tau)},$$

to ensure that the objective function is non-increasing in each iteration.

The algorithm iteratively updates $\mathbf{v}_{\text{PS}}^\tau$ and η^τ until convergence, ensuring a critical point to the problem. The proposed method to optimize is given in Algorithm 2. Due to convexity of (23), it is guaranteed that Algorithm 2 converges to a stationary solution [35].

APPENDIX E RCG METHOD FOR ANALOG COMBINING

Similar to Appendix D, we use the RCG method to optimize phase rotations of analog combiners at users. The user combiner can be partially or fully-connected. The problem with respect to analog combining is separable across users. Therefore, optimizing with respect to different combiners can be done in parallel. The Euclidean gradient at $\mathbf{U}_{\text{RF},k}^\tau$ is

$$\begin{aligned} & \nabla \text{tr}(\mathbf{W}_k^s \mathbf{E}_k^s) \\ &= \sum_{s \in \mathcal{S}} \mathbf{H}_k^s \mathbf{V}_{\text{RF}} \left(\sum_{j=1}^K \mathbf{V}_j^s \mathbf{V}_j^{s^H} \right) \mathbf{V}_{\text{RF}}^H \mathbf{H}_k^{s^H} \mathbf{U}_{\text{RF},k} \mathbf{U}_k^s \mathbf{W}_k^s \mathbf{U}_k^{s^H} \\ & \quad - \mathbf{H}_k^s \mathbf{V}_{\text{RF}} \mathbf{V}_k^s \mathbf{W}_k^s \mathbf{U}_k^{s^H}. \end{aligned} \quad (31)$$

The steps of the RCG algorithm are as follows. In order to obtain $\mathbf{U}_{\text{RF},k}^{\tau+1}$, we perform Armijo backtracking line search to obtain α_1 . Then, $\mathbf{U}_{\text{RF},k}^{\tau+1}$ is obtained as

$$\mathbf{U}_{\text{RF},k}^{\tau+1} = \text{Retr}_{\mathbf{U}_{\text{RF},k}^\tau}(\alpha_1 \eta^\tau) = \text{matrix} \left[\left\{ \frac{\mathbf{U}_{\text{RF},k}^\tau[i,j] + \alpha_1 \eta^\tau[i,j]}{|\mathbf{U}_{\text{RF},k}^\tau[i,j] + \alpha_1 \eta^\tau[i,j]|} \right\}_{i,j} \right],$$

where the operator matrix $[\cdot]$ builds a new matrix where each entry $[i,j]$ is given by the above argument. The Riemannian gradient is then

$$\zeta_{\mathbf{U}_{\text{RF},k}}(\mathbf{U}_{\text{RF},k}^\tau) = \nabla \text{tr}(\mathbf{W}_k^s \mathbf{E}_k^s) - \Re\{\nabla \text{tr}(\mathbf{W}_k^s \mathbf{E}_k^s) \odot \mathbf{U}_{\text{RF},k}^{\tau*} \} \odot \mathbf{U}_{\text{RF},k}^\tau.$$

If the user structure is partially connected, the above equation is applied to non-zero entries only. We compute new Polak-Ribiere parameter α_2 as follows:

$$\alpha_2 = \frac{\text{tr}(\zeta_{\mathbf{U}_{\text{RF},k}}(\mathbf{U}_{\text{RF},k}^{\tau+1})^H(\zeta_{\mathbf{U}_{\text{RF},k}}(\mathbf{U}_{\text{RF},k}^{\tau+1}) - \zeta_{\mathbf{U}_{\text{RF},k}}(\mathbf{U}_{\text{RF},k}^\tau)))}{\text{tr}(\zeta_{\mathbf{U}_{\text{RF},k}}(\mathbf{U}_{\text{RF},k}^\tau)^H \zeta_{\mathbf{U}_{\text{RF},k}}(\mathbf{U}_{\text{RF},k}^\tau))}.$$

Similar to the previous section, the next iterate $\eta^{\tau+1}$ can be obtained as follows:

$$\eta^{\tau+1} = -\zeta_{\mathbf{U}_{\text{RF},k}}(\mathbf{U}_{\text{RF},k}^{\tau+1}) + \alpha_2(\eta^\tau - \Re\{\eta^\tau \odot \mathbf{U}_{\text{RF},k}^{\tau+1}\} \odot \mathbf{U}_{\text{RF},k}^{\tau+1}).$$

The initial search direction is set as $\eta^0 = -\zeta_{\mathbf{U}_{\text{RF},k}}(\mathbf{U}_{\text{RF},k}^0)$. We iteratively update $\eta^{\tau+1}$ and $\mathbf{U}_{\text{RF},k}^{\tau+1}$ until both blocks converge. The convergence proof of this method is similar to the previous section.

APPENDIX F COMPLEXITY ANALYSIS

In this section, we consider the complexity of the sequential optimization. The per-iteration complexity of the BCD-based RF precoding to update one PS value is $\mathcal{O}(N_t)$ and to update all variables once is $\mathcal{O}(N_t^2)$. The per-iteration complexity of the RCG-based RF precoding (given in the appendix) is $\mathcal{O}(N_t^2)$, since the most computationally intensive step is the calculation of the Euclidean gradient, which is dominated by the matrix-vector product in (29), where \mathbf{Q}_{PS} is an $N_t \times N_t$ matrix. The computational complexity of calculating δ_{am}^1 is $\mathcal{O}(S n_k)$, while it is $\mathcal{O}(S n_k^2 N_r^2)$ for δ_{am}^2 . The per-variable BCD-based analog combiner computational complexity is $\mathcal{O}(S n_k^2 N_r^2)$. For the RCG-based user combiner, discussed in the appendix, the matrix multiplications in (31) of the gradient calculation are dominant parts. The overall per-user complexity is $\mathcal{O}(S N_r^3)$. The per-iteration per-user complexity of the bisection-search to solve the digital precoder subproblem in (16) is $\mathcal{O}(N_{\text{RF}}^3 + N_{\text{RF}}^2 n_k)$. This complexity is obtained by performing a single $\mathcal{O}(N_{\text{RF}}^3)$ inversion of the $N_{\text{RF}} \times N_{\text{RF}}$ matrix, and then a matrix multiplication at a cost of $\mathcal{O}(N_{\text{RF}}^2 n_k)$. The per-user per-subcarrier computation complexity of (18) is $\mathcal{O}(N_{\text{RF}} S K n_k)$. The same per-user per-subcarrier computational complexity holds for (20).